Spiral and Elliptical Galaxies: what are their properties and how did they form?

Disk Galaxies: Observational Facts

Exponential Surface Brightness Profiles

- Disk galaxies have surface brightness profiles that often are close to exponential.
- Deviations from exponential at small radii are attributed to bulge and/or bar.
- Deviations from exponential at large radii are attributed to star formation thresholds, radial migration, and/or maximum angular momentum...

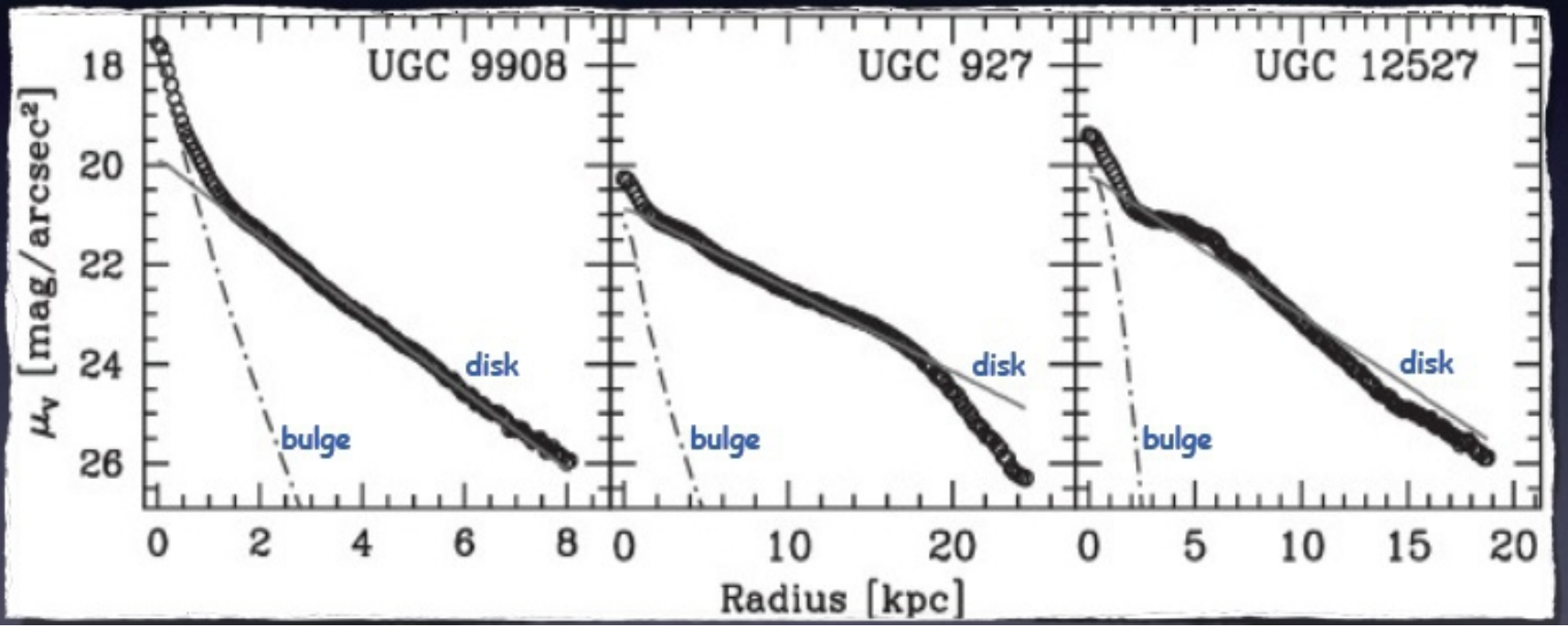

Disk Galaxies: Observational Facts

Flat Rotation Curves

Disk galaxies have flat rotation curves. Unfortunately, it is difficult to obtain unique disk-halo(-bulge) decompositions....

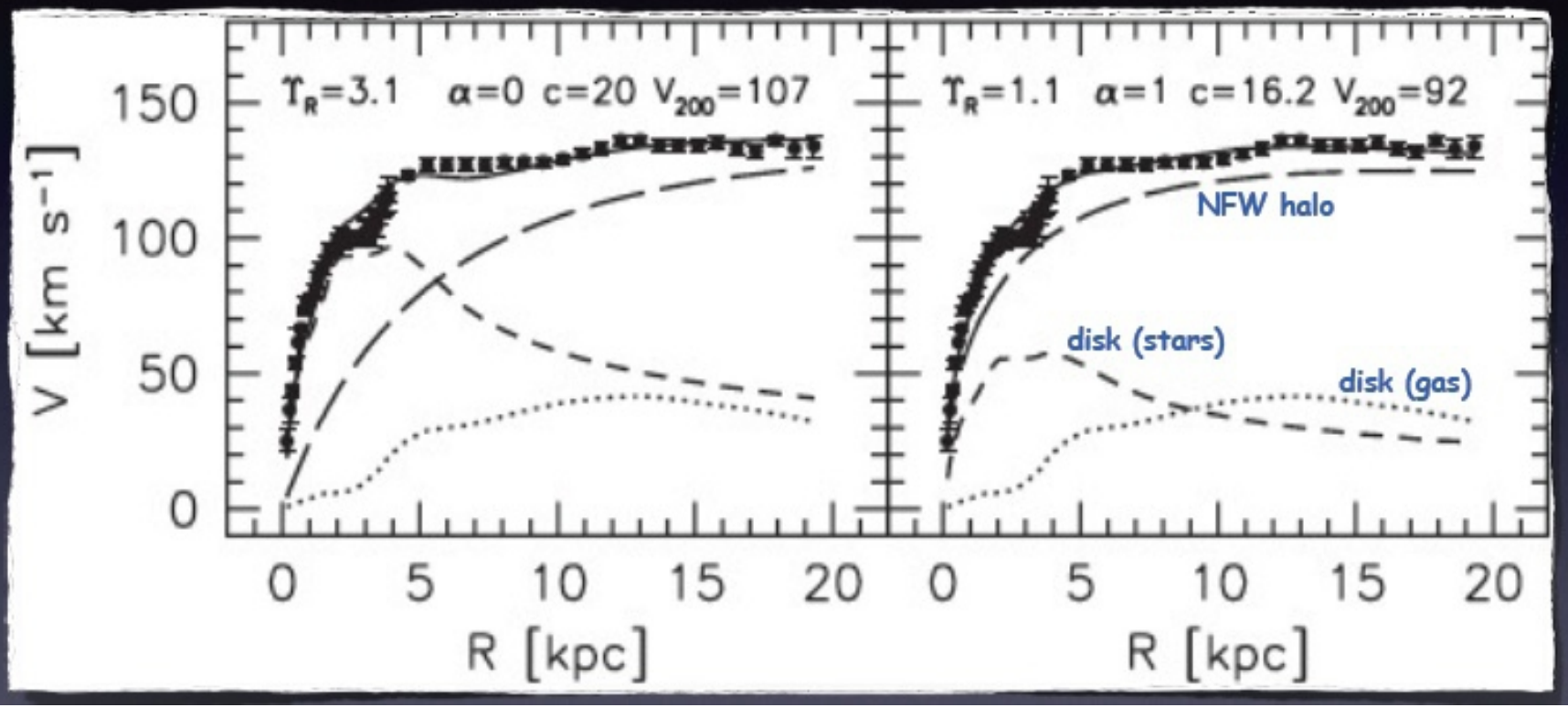

Disk Galaxies: Observational Facts

Exponential Surface Brightness Profiles

Because of their close-to-exponential appearance, disk galaxies are often modelled as infinitesimally thin, exponential disks:

surface brightness $I(R) = I_0\,\mathrm{e}^{-R/R_\mathrm{d}}$ $L_\mathrm{d} = 2\pi \int_0^\infty I(R)\,R\,\mathrm{d}R = 2\pi\,I_0\,R_\mathrm{d}^2$

surface mass density $\Sigma(R) = \Sigma_0\,\mathrm{e}^{-R/R_\mathrm{d}}$ $M_\mathrm{d} = 2\pi \int_0^\infty \Sigma(R)\,R\,\mathrm{d}R = 2\pi\,\Sigma_0\,R_\mathrm{d}^2$

circular velocity $V_{\mathrm{c,d}}^2(R) = -4\pi G\Sigma_0\,R_\mathrm{d}^2\,y\,[I_0(y)\,K_0(y) - I_1(y)\,K_1(y)]$

disk scale length R_d stellar mass-to-light ratio $M_\mathrm{d}/L_\mathrm{d} = \Sigma_0/I_0$

$y \equiv R/(2\,R_\mathrm{d})$ modified Bessel functions $I_n(x)$ $K_n(x)$

The circular velocity curve reaches a maximum at $R \simeq 2.16\,R_\mathrm{d}$

Disk Galaxies: Observational Facts

Scaling Relations

Brighter disks

- are larger
- are redder
- have higher central SB
- have smaller gas mass fractions
- rotate faster (Tully-Fisher relation)

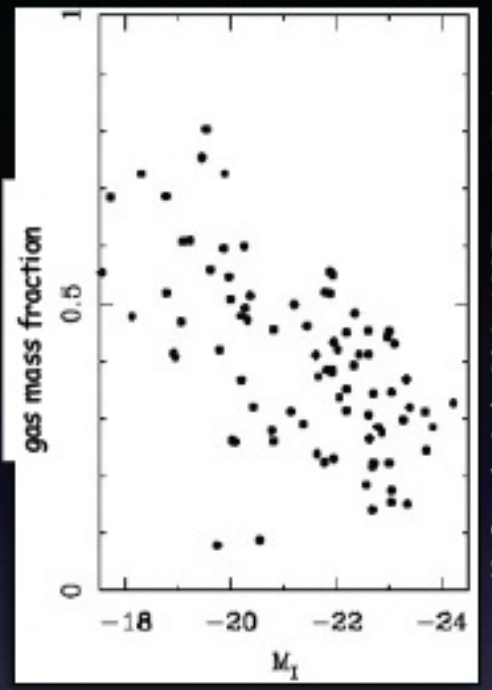

McGaugh & de Blok, 1997, ApJ, 534, 146

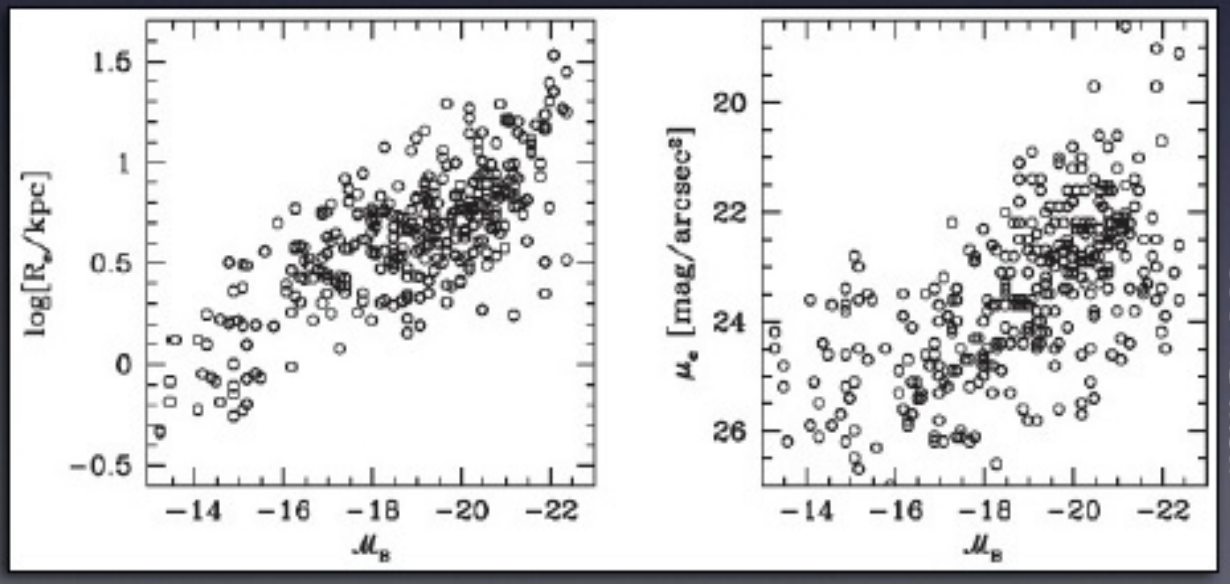

MBW, Fig. 2.20

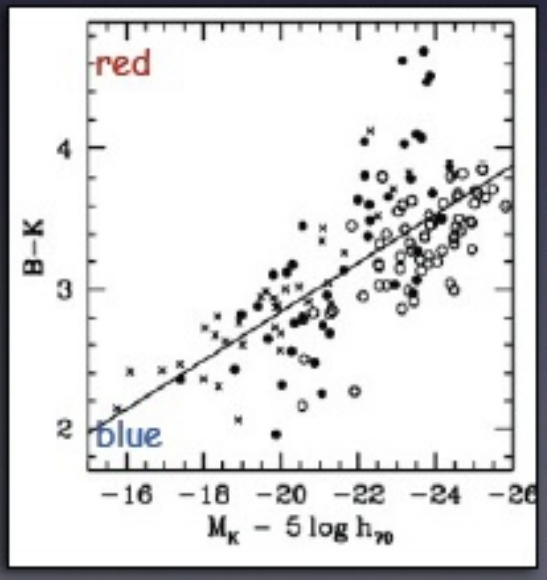

vdBosch & Dalcanton, 2000, ApJ, 534, 146

Tully–Fisher relation

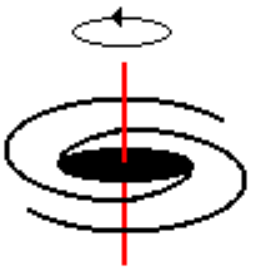

spiral galaxies rotate, and the rotation speed is proportional to the mass of the galaxy

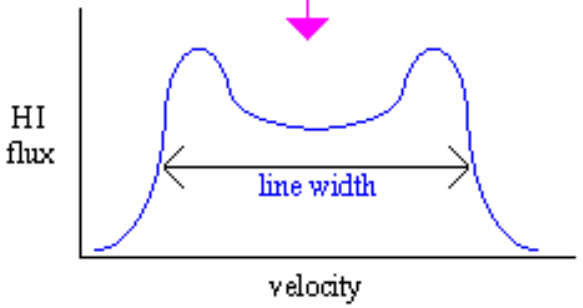

measurements of neutral hydrogen (HI) display a ''double–horned'' profile, where the width of the line indicates the mass

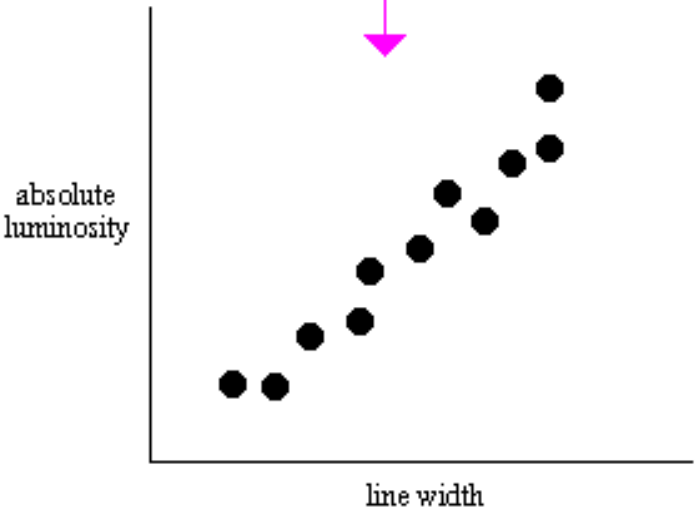

a plot of line width versus absolute luminosity of a galaxy is called the Tully–Fisher relation. When calibrated using galaxies with Cepheid distances, the TF relation is used to determine Hubble's constant.

Tully-Fisher Relation in different Photometric Bands

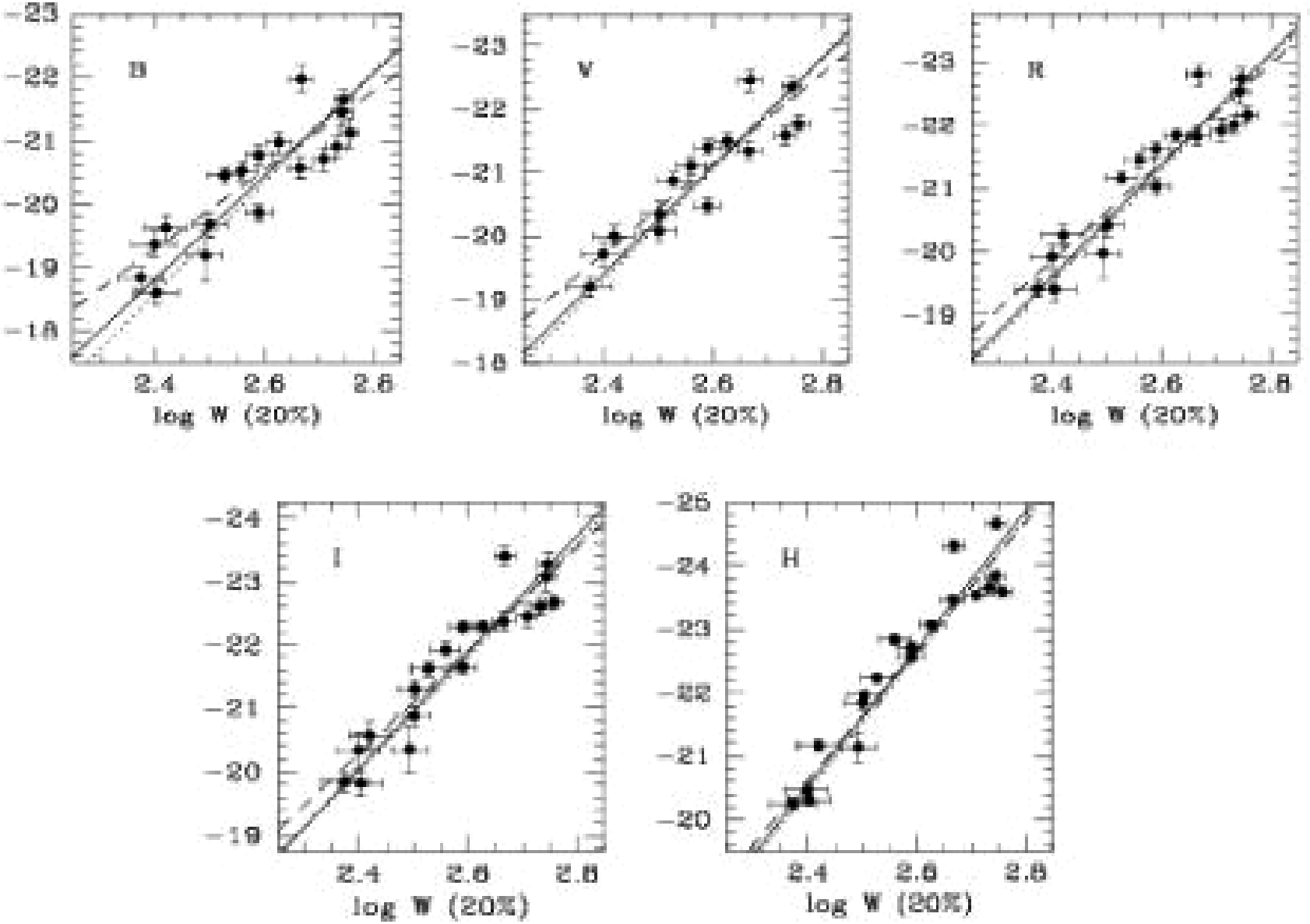

Stellar mass as a function of circular velocity

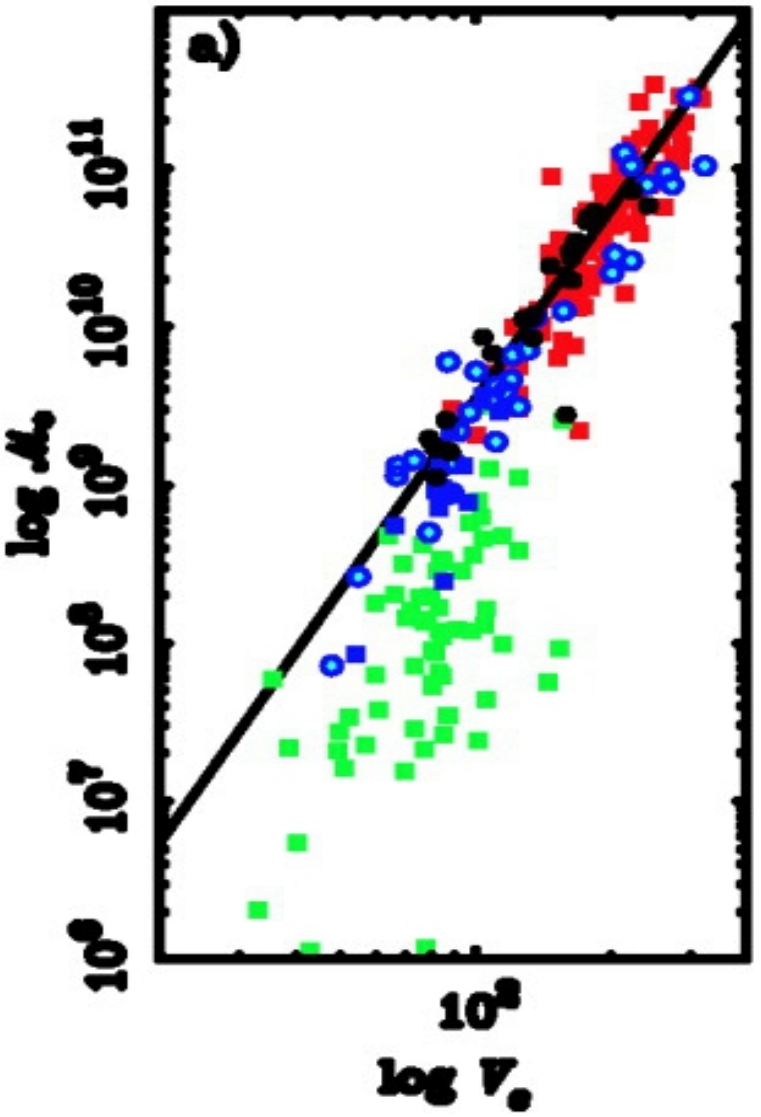

Stellar + gas (baryonic) mass as a function of circular velocity

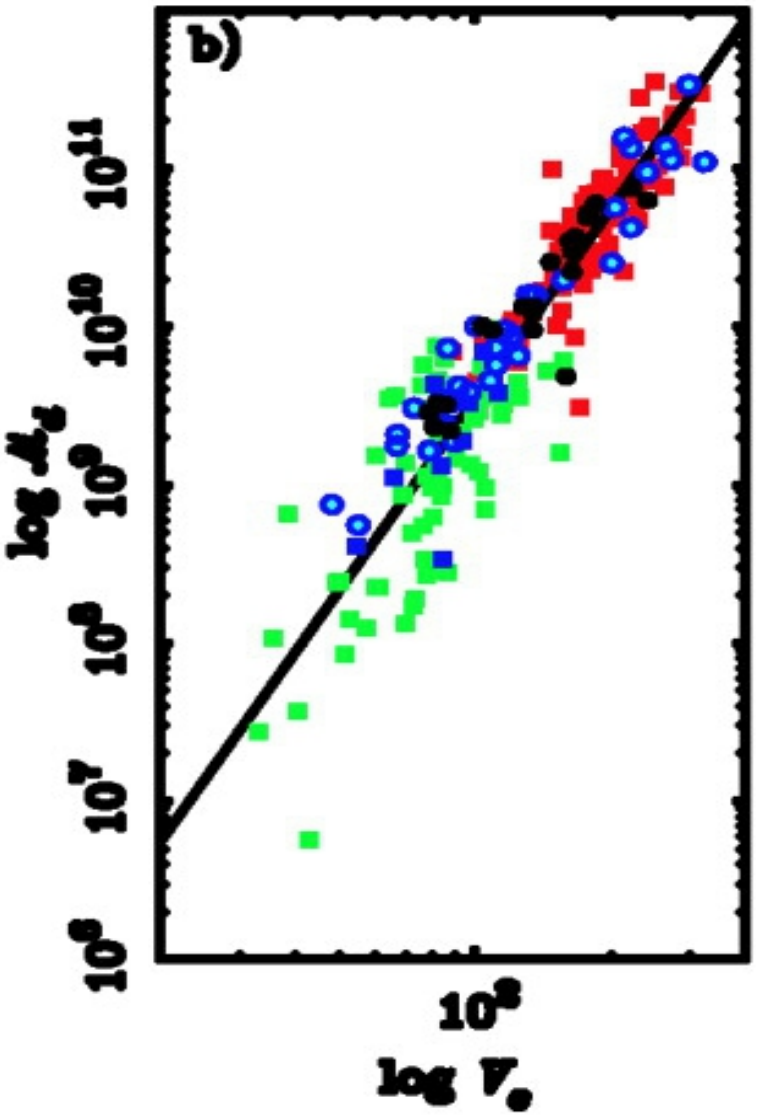

Linear Tidal Torque Theory

See MBW §7.5.4 for more details

Dark matter haloes acquire angular momentum in the linear regime due to tidal torques from neighboring overdensities...

Consider the material that ends up as part of a virialized halo. Let V_L be the Lagrangian region that it occupies in the early Universe. The angular momentum of this material can be written as

$$\vec{J} = \int_{V_L} \mathrm{d}^3\vec{x}_\mathrm{i}\, \bar{\rho}_\mathrm{m} a^3 \left(a\vec{x} - a\vec{x}_\mathrm{com}\right) \times \vec{v}$$

where $\vec{x}_\mathrm{com}$ is the center of mass (the barycenter) of the volume.

Using the Zel'dovich approximation for the velocities $\vec{v}$ inside the volume, and second-order Taylor series expansion of the potential, one finds that

$$J_i(t) = a^2(t)\, \dot{D}(t)\, \epsilon_{ijk} T_{jl}\, I_{lk}$$

Einstein summation convention

Here $\dot{D}(t)$ is the time-derivative of the linear-growth rate, T_{ij} is the tidal tensor at the barycenter at the initial time, I_{ij} is the inertial tensor at the initial time, and ϵ_{ijk} is the 3D Levi-Civita tensor (also called the completely antisymmetric tensor)

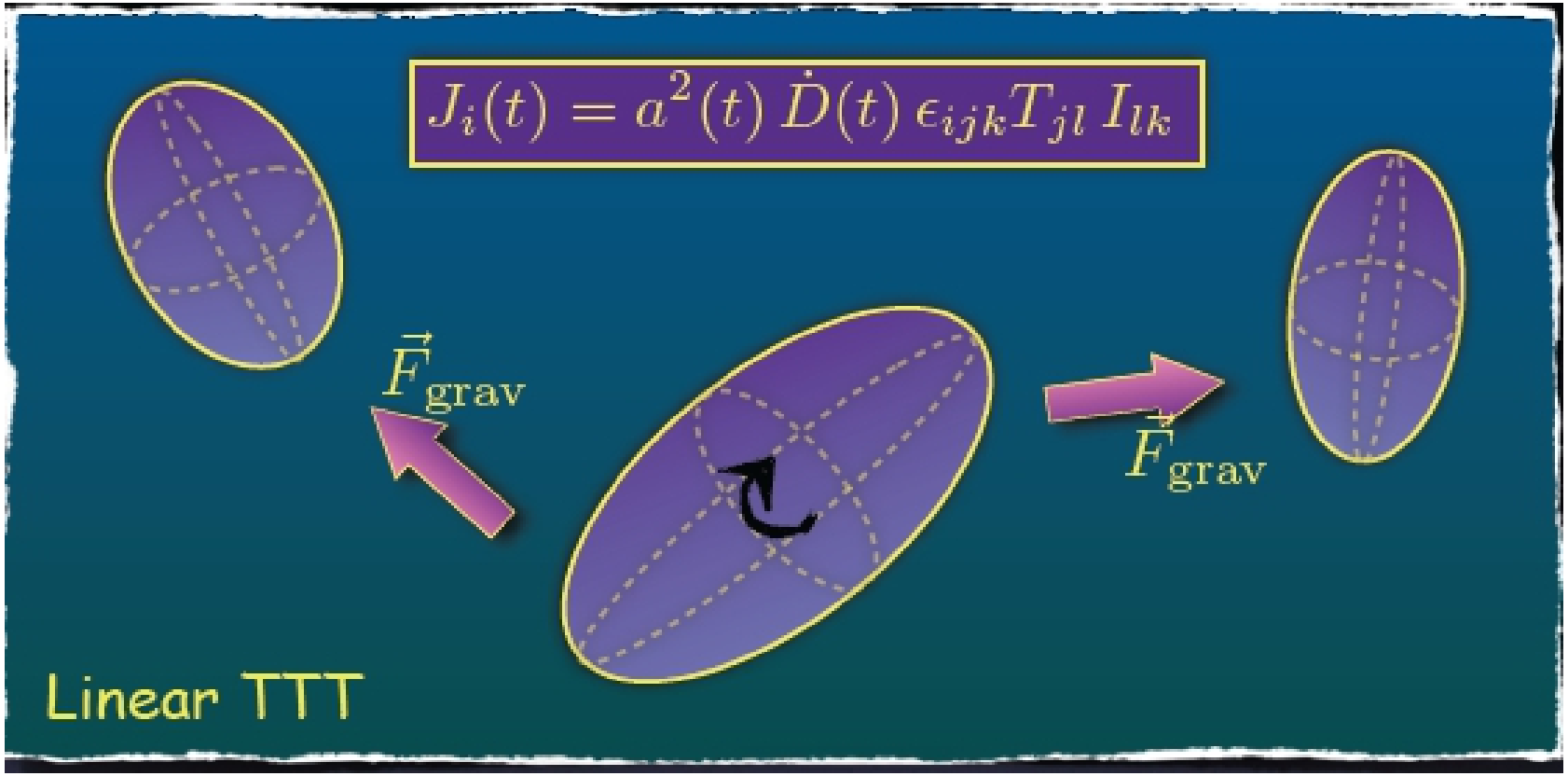

According to linear TTT, the acquisition of angular momentum stops once a proto-halo turns around and starts to collapse: after turn-around, the moment of inertia starts to decline rapidly...Hence, according to linear TTT the final angular momentum of a virialized dark matter halo should (roughly) be equal to

$$J_{\rm vir} = \int_0^{t_{\rm ta}} J(t)\,{\rm d}t = \epsilon_{ijk}\,T_{jl}\,I_{lk} \int_0^{t_{\rm ta}} a^2(t)\,\dot{D}(t)\,{\rm d}t$$

The Halo Spin Parameter

The angular momentum of a dark matter halo is traditionally parameterized through the dimensionless spin parameter:

$$\lambda = \frac{J\,|E|^{1/2}}{G\,M^{5/2}}$$

where J, E and M are the angular momentum, energy and mass of the halo.

An alternative definition for the spin parameter, which avoids having to calculate the halo energy is:

$$\lambda' = \frac{J}{\sqrt{2}M\,V\,R}$$

where V and R are the virial velocity and viral radius, respectively. Definitions are equal if halo is singular isothermal sphere; otherwise they differ by factor of order unity....

Simulations show that PDF for spin parameter of haloes is a log-normal

$$\mathcal{P}(\lambda)\,\mathrm{d}\lambda = \frac{1}{\sqrt{2\pi}\,\sigma_{\ln\lambda}}\exp\left(-\frac{\ln^2(\lambda/\bar{\lambda})}{2\sigma^2_{\ln\lambda}}\right)\frac{\mathrm{d}\lambda}{\lambda}$$

with $\bar{\lambda} \simeq 0.03$ and $\sigma_{\ln\lambda} \simeq 0.5$, with virtually no dependence on halo mass or cosmology...

The Formation of Disk Galaxies

Hot (shock-heated) gas inside extended dark matter halo cools radiatively,

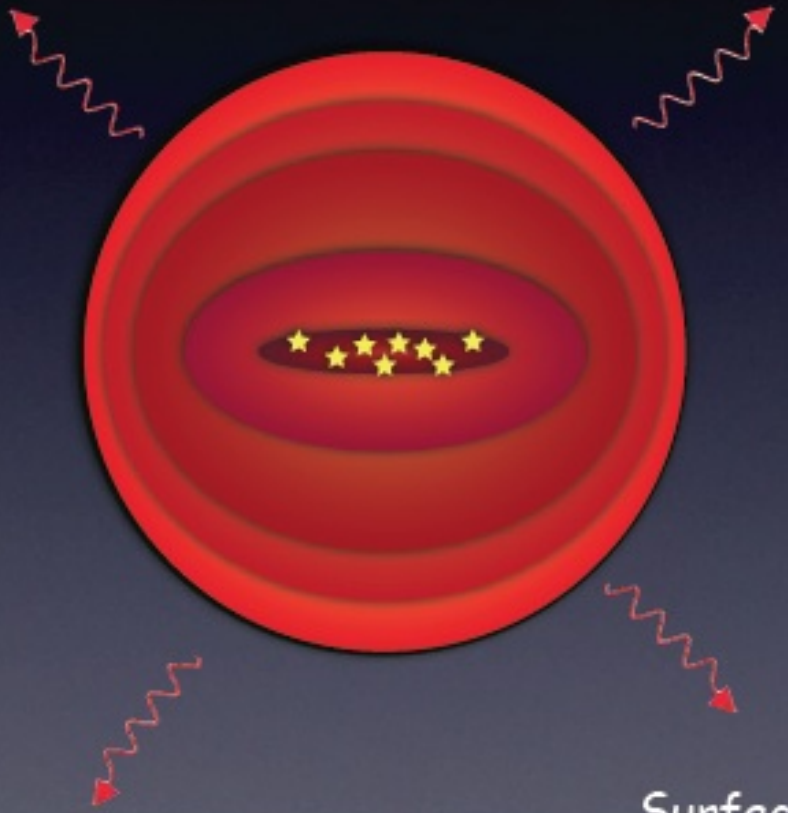

As gas cools, its pressure decreases causing the gas to contract

Since emission of photons is isotropic, angular momentum of cooling gas is conserved.

As gas sphere contracts, it spins up, and flattens

Surface density of disk increases, `triggering' star formation; a disk galaxy is born...

Simple Model to Predict Disk Sizes and Rotation Curves From Dark Halo Properties plus assumption that Gas Conserves Angular Momentum

For a singular isothermal sphere the density profile is just

$$\rho(r) = \frac{V_c^2}{4\pi G r^2}, \tag{1}$$

we define the limiting radius of a dark halo to be the radius r_{200} within which the mean mass density is $200\rho_{crit}$, where ρ_{crit} is the critical density for closure at the redshift z when the halo is identified. Thus, the radius and mass of a halo of circular velocity V_c seen at redshift z are

$$r_{200} = \frac{V_c}{10H(z)}; \quad M = \frac{V_c^2 r_{200}}{G} = \frac{V_c^3}{10GH(z)}, \tag{2}$$

where

$$H(z) = H_0\left[\Omega_{\Lambda,0} + (1 - \Omega_{\Lambda,0} - \Omega_0)(1+z)^2 + \Omega_0(1+z)^3\right]^{1/2} \tag{3}$$

is the Hubble constant at redshift z.

We assume that the mass which settles into the disc is a fixed fraction m_d of the halo mass. The disc mass is then

$$M_d = \frac{m_d V_c^3}{10GH(z)} \approx 1.7\times 10^{11} h^{-1}\,\mathrm{M}_\odot \left(\frac{m_d}{0.05}\right)\left(\frac{V_c}{250\,\mathrm{km\,s^{-1}}}\right)^3 \left[\frac{H(z)}{H_0}\right]^{-1}.$$

Let us **assume** an exponential profile for the disk:

$$\Sigma(R) = \Sigma_0 \exp\left(-R/R_d\right). \tag{5}$$

Here R_d and Σ_0 are the disc scalelength and central surface density, and are related to the disc mass through

$$M_d = 2\pi\Sigma_0 R_d^2. \tag{6}$$

If the gravitational effect of the disc is neglected, its rotation curve is flat at the level V_c and its angular momentum is just

$$J_d = 2\pi \int V_c \Sigma(R) R^2 \mathrm{d}R = 4\pi\Sigma_0 V_c R_d^3 = 2M_d R_d V_c. \tag{7}$$

We assume this angular momentum to be a fraction j_d of that of the halo, i.e.

$$J_d = j_d J, \tag{8}$$

and we relate J to the spin parameter λ of the halo through the definition

$$\lambda = J|E|^{1/2} G^{-1} M^{-5/2}, \tag{9}$$

where E is the total energy of the halo. Equations (7) and (8) then imply that

$$R_d = \frac{\lambda G M^{3/2}}{2V_c|E|^{1/2}}\left(\frac{j_d}{m_d}\right). \tag{10}$$

The total energy of a truncated singular isothermal sphere is easily obtained from the virial theorem by assuming all particles to be on circular orbits:

$$E = -\frac{GM^2}{2r_{200}} = -\frac{MV_c^2}{2}. \tag{11}$$

On inserting this into equation (10) and using equations (2) and (6) we get

$$R_d = \frac{1}{\sqrt{2}}\left(\frac{j_d}{m_d}\right)\lambda r_{200}$$

$$\approx 8.8h^{-1}\,\mathrm{kpc}\left(\frac{\lambda}{0.05}\right)\left(\frac{V_c}{250\,\mathrm{km\,s^{-1}}}\right)\left[\frac{H}{H_0}\right]^{-1}\left(\frac{j_d}{m_d}\right), \tag{12}$$

and

$$\Sigma_0 \approx 4.8\times 10^{22} h\,\mathrm{cm^{-2}} m_H \left(\frac{m_d}{0.05}\right)\left(\frac{\lambda}{0.05}\right)^{-2}$$

$$\times\left(\frac{V_c}{250\,\mathrm{km\,s^{-1}}}\right)\left[\frac{H(z)}{H_0}\right]\left(\frac{m_d}{j_d}\right)^2, \tag{13}$$

where m_H is the mass of a hydrogen atom.

approximate the distribution of λ by

$$p(\lambda)\,d\lambda = \frac{1}{\sqrt{2\pi}\sigma_\lambda}\exp\left[-\frac{\ln^2(\lambda/\bar{\lambda})}{2\sigma_\lambda^2}\right]\frac{d\lambda}{\lambda}, \qquad (15)$$

where $\bar{\lambda} = 0.05$ and $\sigma_\lambda = 0.5$. This function is a good fit to the *N*-body results of Warren et al. (1992; see also Cole & Lacey 1996;

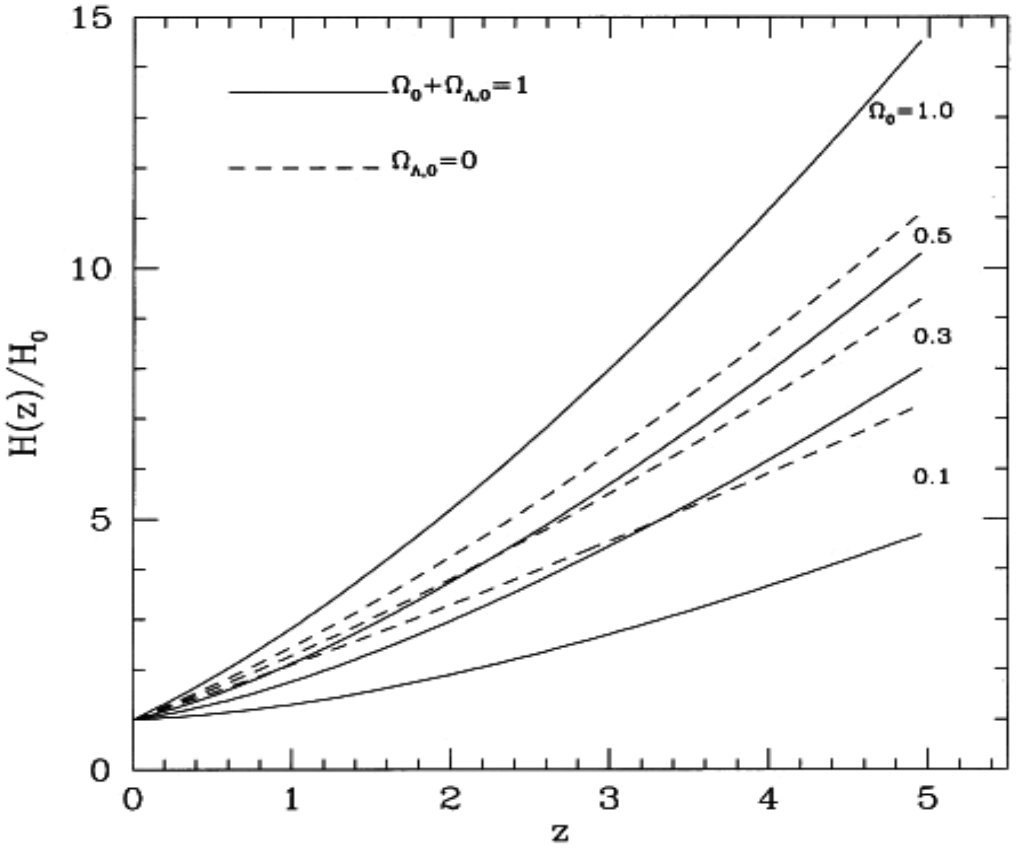

Figure 1. The Hubble constant (in units of its present value) as a function of redshift for flat ($\Omega_0 + \Omega_{\Lambda,0} = 1$) and open models with various Ω_0.

Sizes of Disk Galaxies and their Evolution

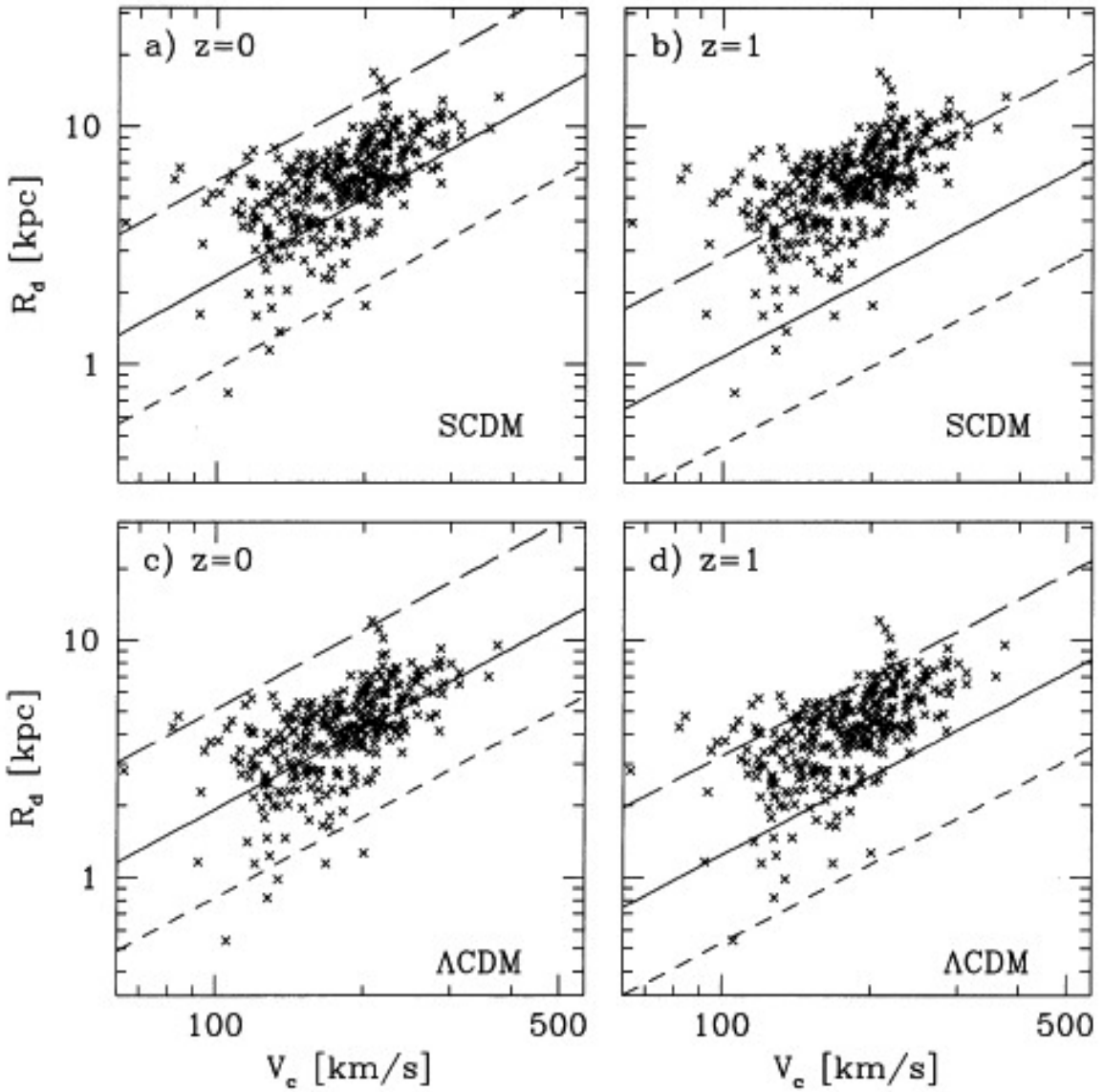

Figure 4. Model predictions for R_d as a function of V_c for stable discs assembled at $z = 0$ and at $z = 1$ in the SCDM and ΛCDM models. The solid lines give the relations for critical discs when $m_d = 0.05$, while short-dashed lines give the corresponding relations for $m_d = 0.025$. Stable discs must lie above the line for the relevant value of m_d. The long-dashed lines correspond to $m_d = j_d$ and $\lambda = 0.1$; at most 10 per cent of discs should lie above these lines. The data points are the observational results of Courteau (1996, 1997) for a sample of nearby normal spirals.

Predicted Rotation Curves: dependence on parameters

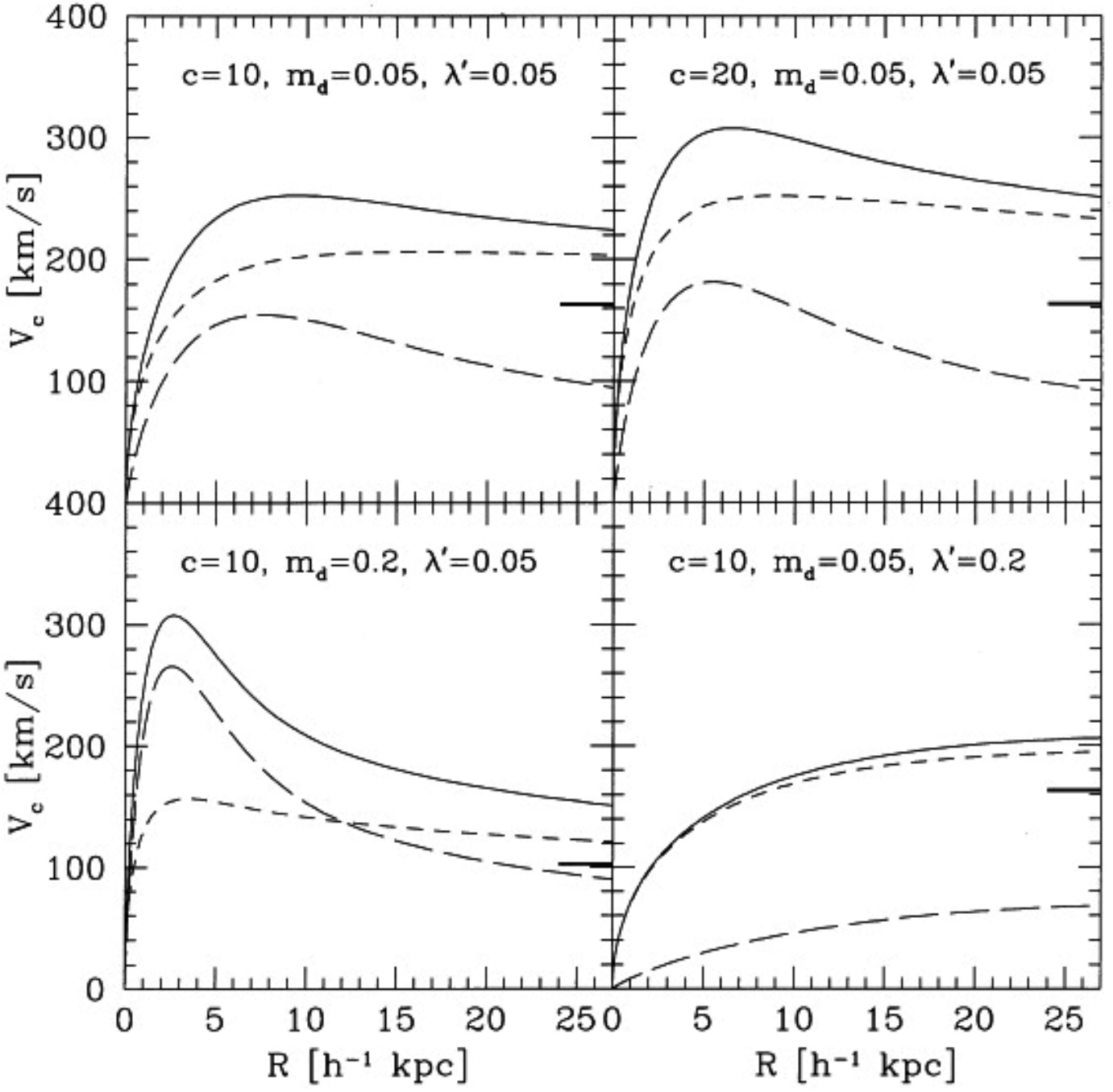

Theoretically predicted Tully-Fisher Relations

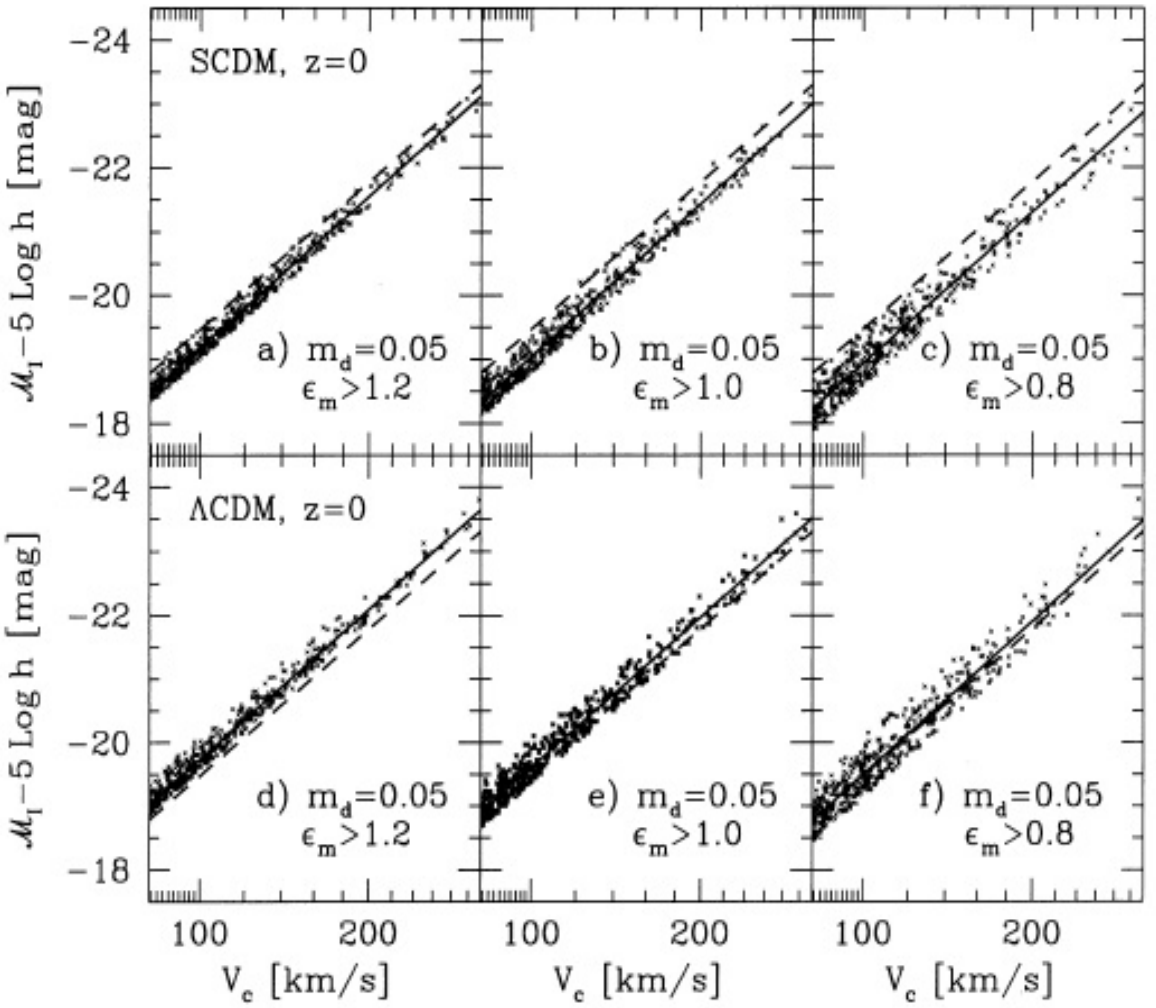

Figure 6. Tully–Fisher (TF) relations for stable discs at $z = 0$ in the SCDM and ΛCDM cosmogonies. Monte Carlo samples of the predicted luminosity–rotation velocity distribution are shown for three choices of ϵ_m. We have converted stellar mass (in the model) into *I*-band luminosity using $\Upsilon = 1.7h$ (Bottema 1997). The solid lines give the linear regressions of absolute magnitude against log V_c. The dashed lines show the observed TF relation as given by Giovanelli et al. (1997).

Barred Spirals

NGC 1365

NGC 1300

Local Disk Stability: Toomre's Q Parameter

- When are self-gravitating disks vulnerable to **local** gravitational instabilities ?

  Instabilities can arise from a competition between:

  - gravity causing overdense regions to collapse
  - stellar dispersion which inhibits the collapse
  - angular momentum which inhibits the collapse

  Toomre (1964) found the conditions for instability: $Q < 1$ where $Q \approx \kappa \sigma / (3 G \Sigma)$
  Where σ is the stellar velocity dispersion and Σ is the local surface density

- Here's a simplified derivation based on a **modified Jeans analysis**:
  Consider overdense region radius R in a **non-rotating** disk

  - The collapse time is $t_{coll} \sim R / V$ where V ~ gravitational velocity ~ $(G M / R)^{½}$

    So $t_{coll} \sim R / (GM / R)^{½} \sim (R^3 / GM)^{½} \sim (R / G \Sigma)^{½}$ (Σ is surface density)

    The time for stars to escape the region is : $t_{esc} \sim R / \sigma$ (σ is dispersion)

    So collapse occurs if $t_{coll} < t_{esc}$ ie $(R / G \Sigma)^{½} < R / \sigma$

    → The critical size **for stability** due to dispersion is therefore : $R_J < \sigma^2 / G \Sigma$

  - Now consider a **rotating** disk:
    The **local** angular velocity is Oort's constant B
    The region is **stable** if $F_{centrifugal} > F_{gravity}$

    In this case $R B^2 > GM / R^2 = G \Sigma$

    → The critical size **for stability** due to rotation is therefore : $R_{rot} > G \Sigma / B^2$

- Combining these: the disk is **unstable** in the range $R_J < R < R_{rot}$

  And therefore the disk is locally **stable** if $R_J > R_{rot}$

  ie $\sigma^2 / G\Sigma > G\Sigma / B^2$ or $\sigma B / G\Sigma > 1$

  Recall that $B = \kappa^2 / 4\Omega$ and $\kappa \sim 1\text{-}2\,\Omega$ so $B \sim \kappa / 3$

The final condition for disk **stability** is therefore

$$Q \equiv \frac{\sigma |B|}{G\Sigma} \cong \frac{\sigma \kappa}{3G\Sigma} > 1$$

[A similar relation for gravitational stability for a **gas** disk is: $Q \equiv V_s \kappa / 3\,G\Sigma > 1$]

N-body hydrodynamical simulations and the "Angular Momentum Catastrophe"

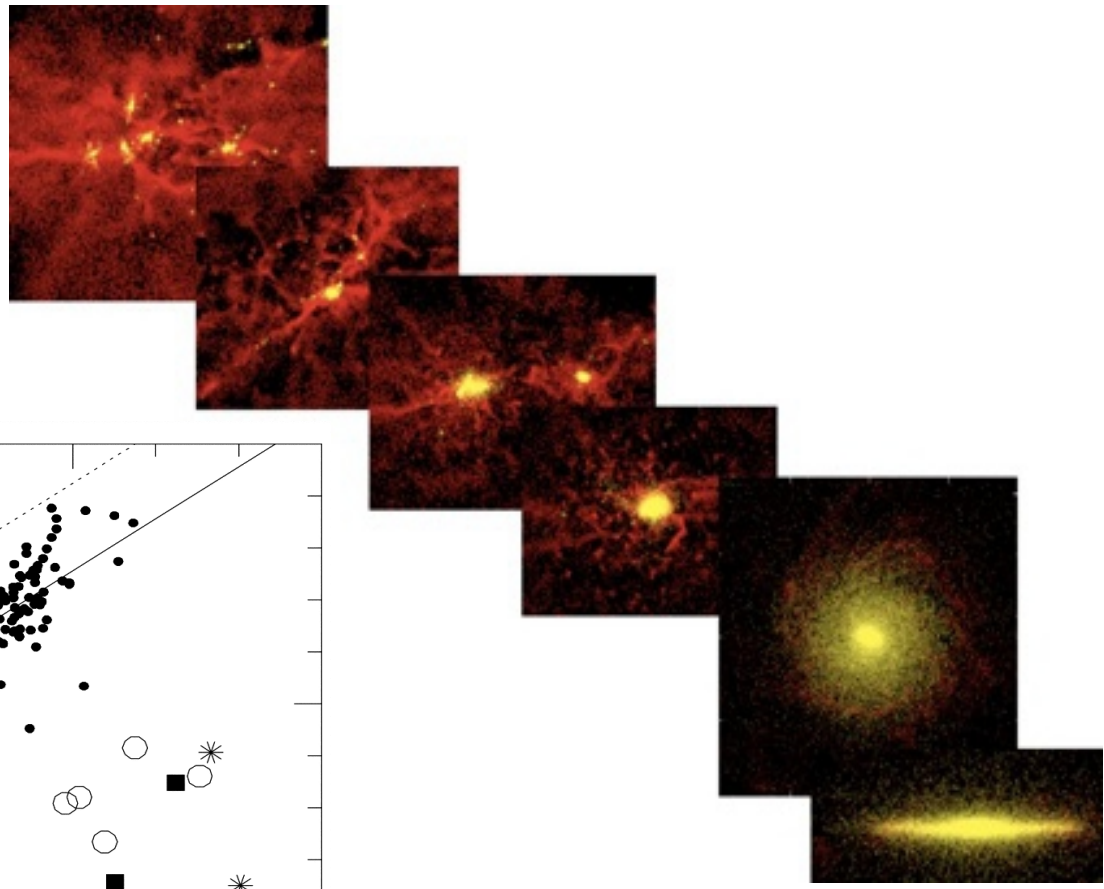

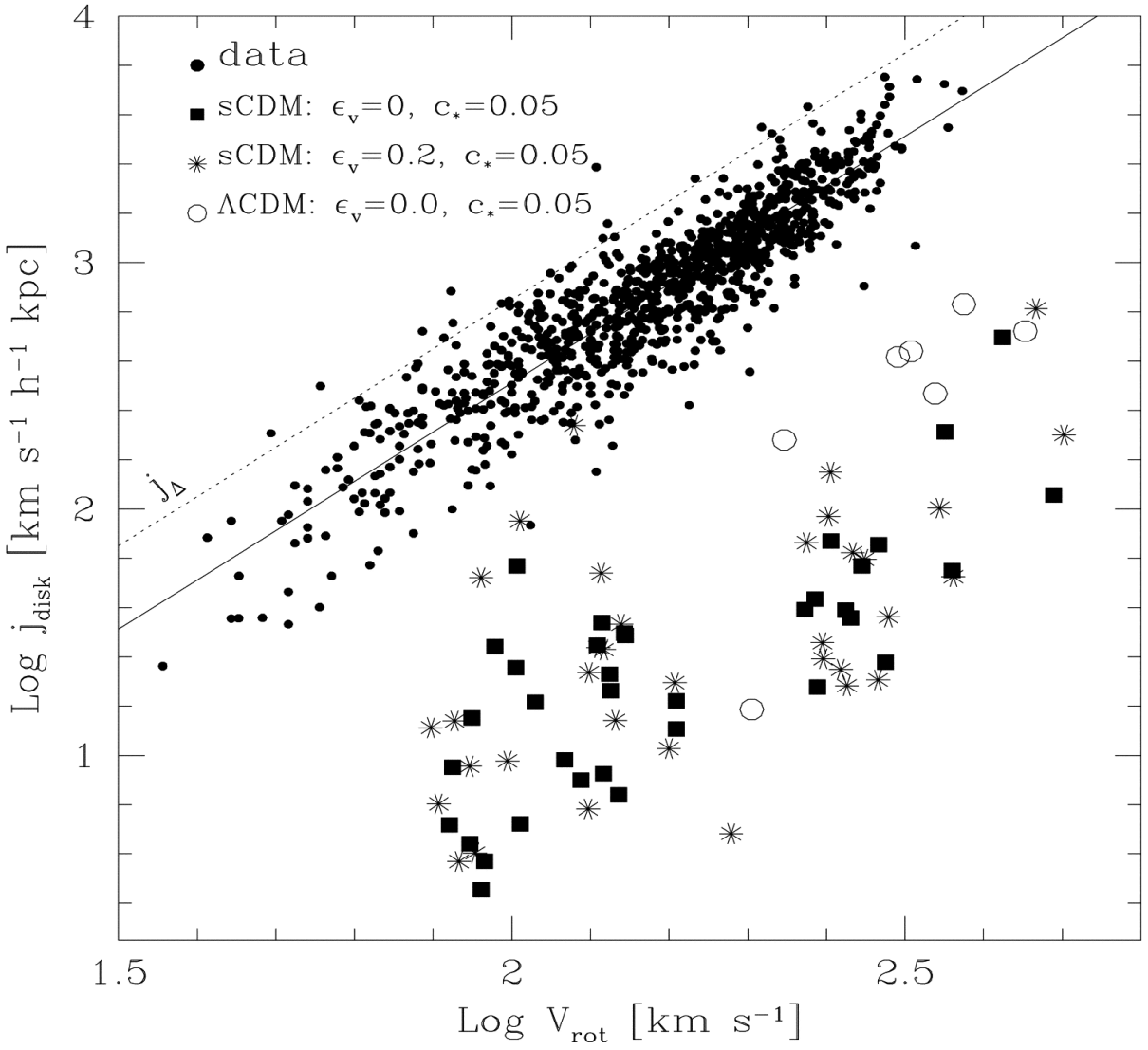

Effect of different supernova feedback implementations on the predicted rotation curves.

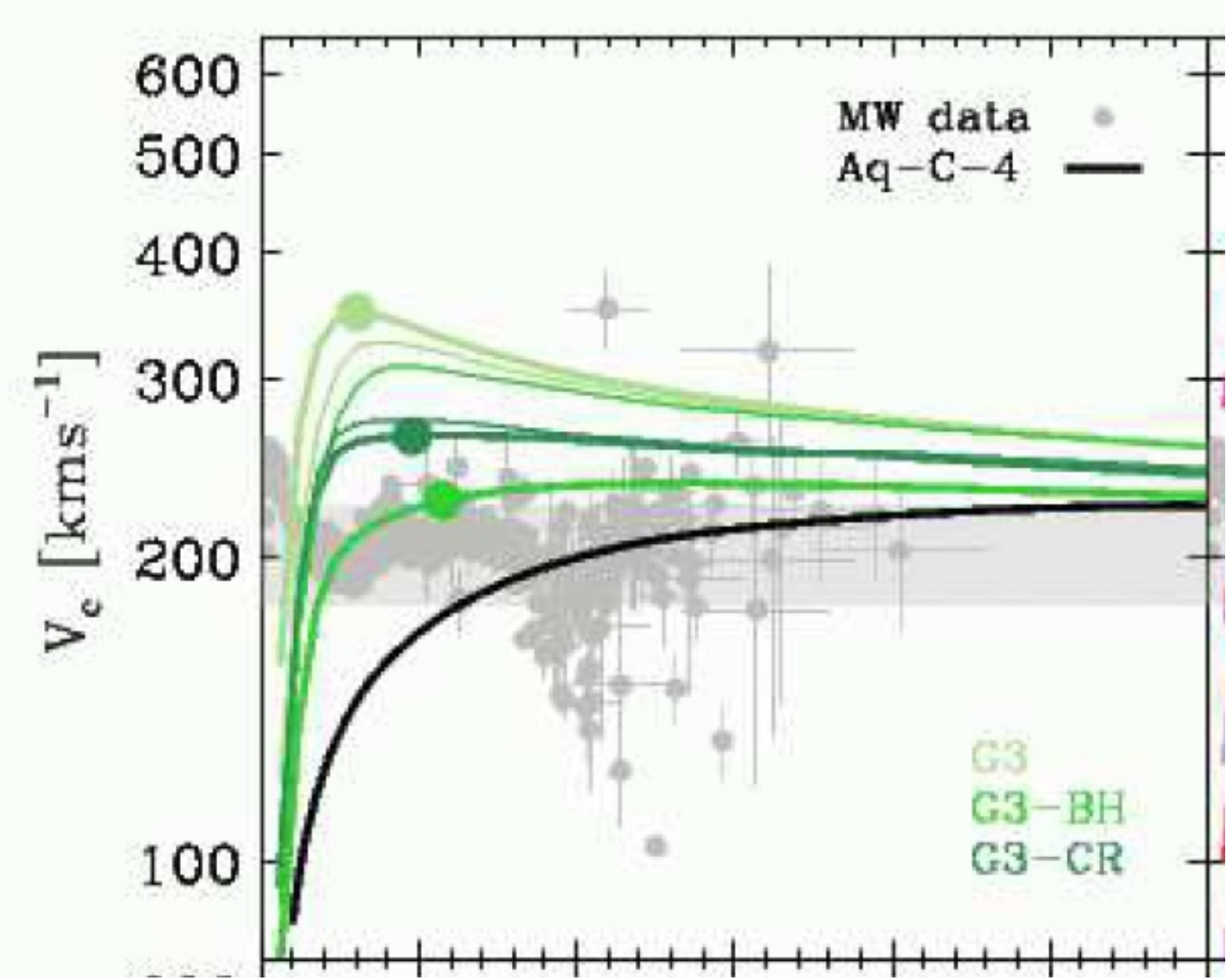













M87 © Anglo-Australian Observatory
Photo by David Malin

(i) deVaucouleurs ($R^{1/4}$) and Sersic ($R^{1/n}$) Laws

deVaucouleurs noticed (1948) that for many ellipticals $\mu \propto R^{1/4}$
The fit is usually good over all but the inner and outermost regions (typically 0.03 - 20 R_e)

The law is usually written :

$$I(R) = I_e \, exp\left(-7.67 \left[(R/R_e)^{1/4} - 1 \right]\right) \qquad (7.3)$$

It has the following properties :

- $L_{tot} = 7.22 \, \pi \, R_e^{\,2} \, I_e$
- $I(0) = 2000 \, I_e$
- $< I(<R_e)> = 3.61 \, I_e$ (which we abbreviate to $< I_e >$ and equivalently $< \mu_e >$)
- Asymptotically, at small R, $I(R) \propto R^{-0.8}$ while at large R, $I(R) \propto R^{-1.7}$
- In terms of surface brightness: $\mu(R) = \mu_e + 8.325[(R/R_e)^{1/4} - 1] = \mu(0) + 8.325 \, (R/R_e)^{1/4}$

The deVaucouleurs law is a special case of a more general, **Sersic** (1963,1968), law:

$$I(R) = I_e \, exp\left(-b \left[(R/R_e)^{1/n} - 1 \right]\right) \qquad (7.4)$$

Where

- b = 1.999 n - 0.327 (n>1) ensures 0.5 $L_{tot} = L(<R_e)$
- n=4 gives the deVaucouleurs $R^{1/4}$ law with b = 7.67
- n=1 gives an exponential profile with b=1.67

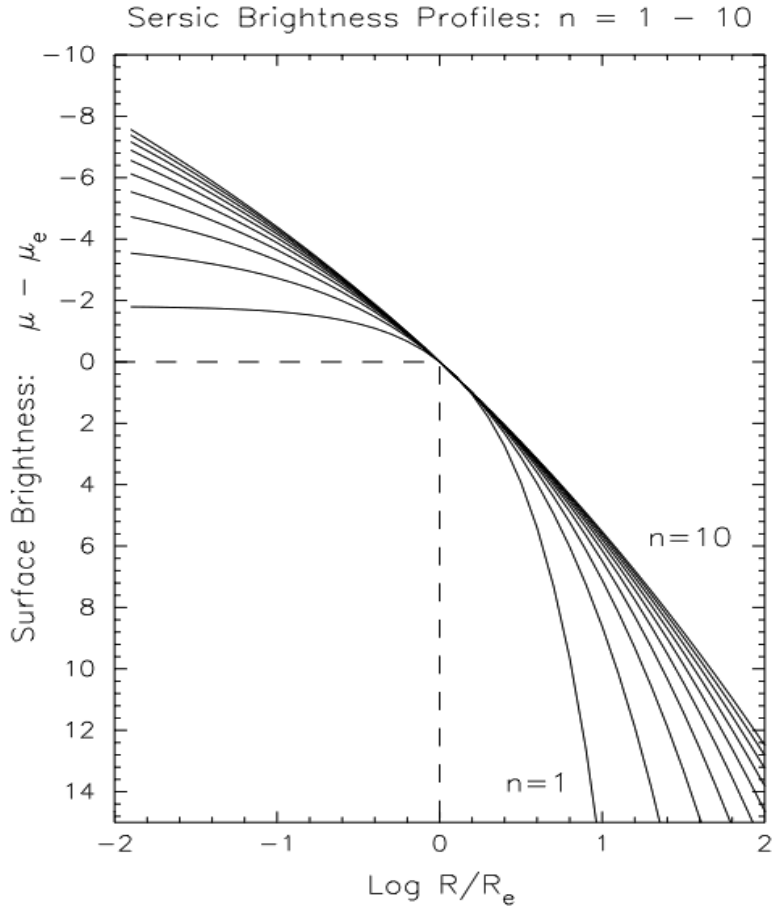

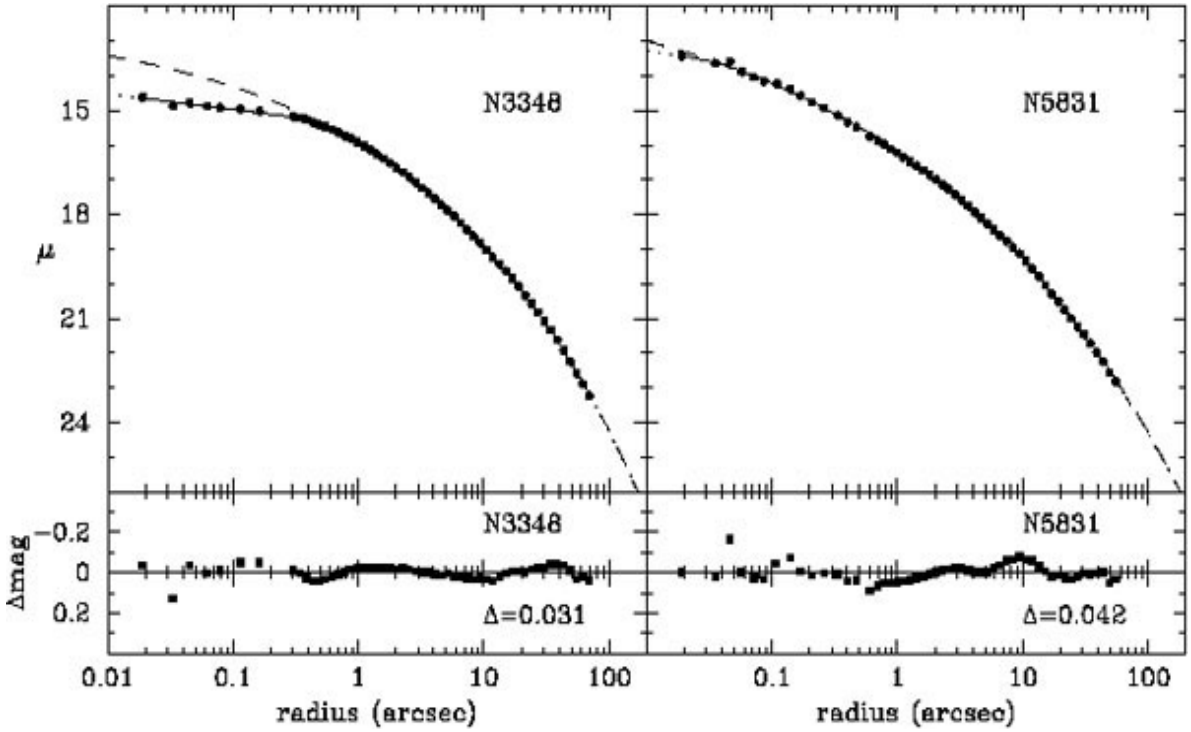

More Luminous E's are More Concentrated

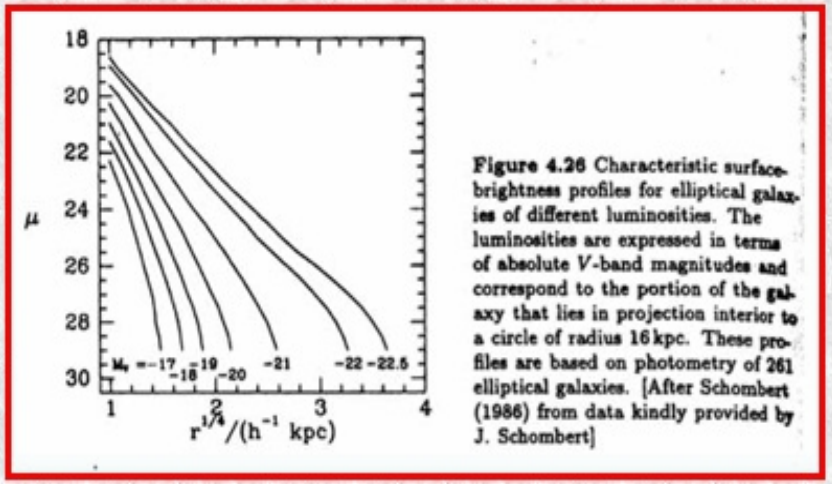

Figure 4.26 Characteristic surface-brightness profiles for elliptical galaxies of different luminosities. The luminosities are expressed in terms of absolute *V*-band magnitudes and correspond to the portion of the galaxy that lies in projection interior to a circle of radius 16 kpc. These profiles are based on photometry of 261 elliptical galaxies. [After Schombert (1986) from data kindly provided by J. Schombert]

Surface brightness profiles for Ellipticals with a range of luminosity. The x axis is $R^{1/4}$ in $kpc^{1/4}$. Clearly, more luminous galaxies are bigger, but also larger n-index since if the profile curves down the n-index is less than 4, but if it curves up it is more than 4.

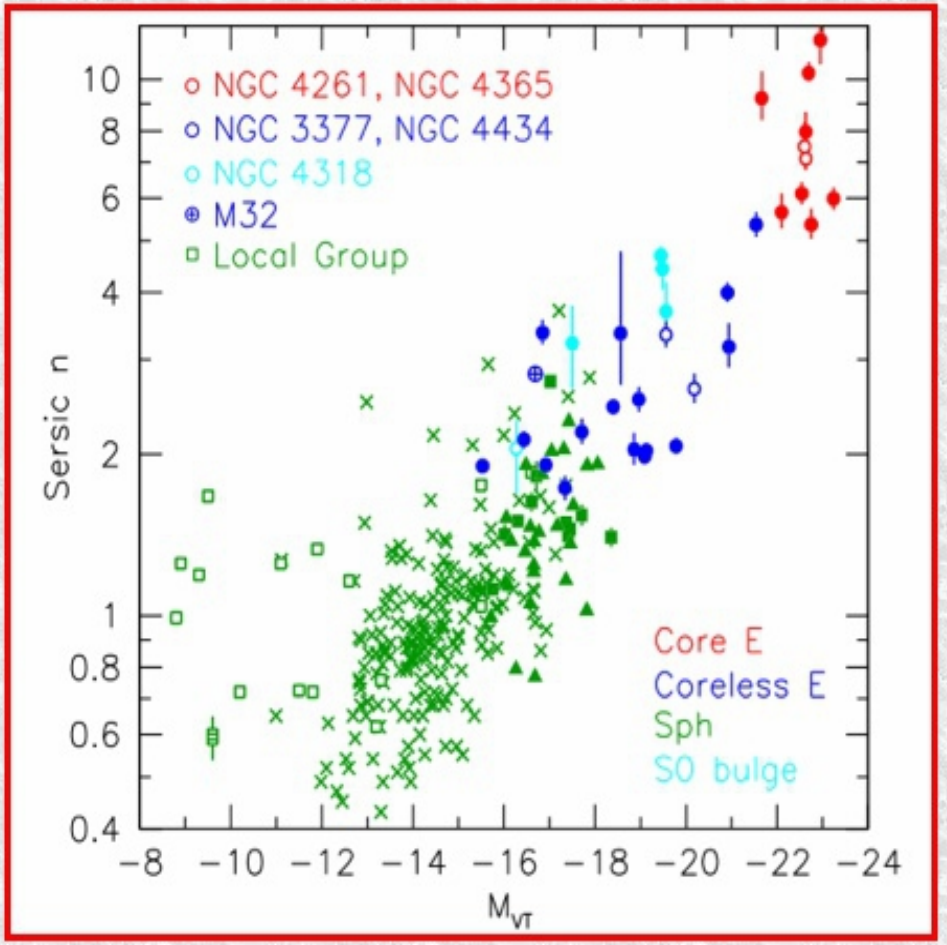

Clear trend for more luminous Elliptical galaxies to have higher n-index (more concentrated profiles). Note the low luminosity dwarf spheroids have Sersic n in the same range as for disks. [Figure 33 from

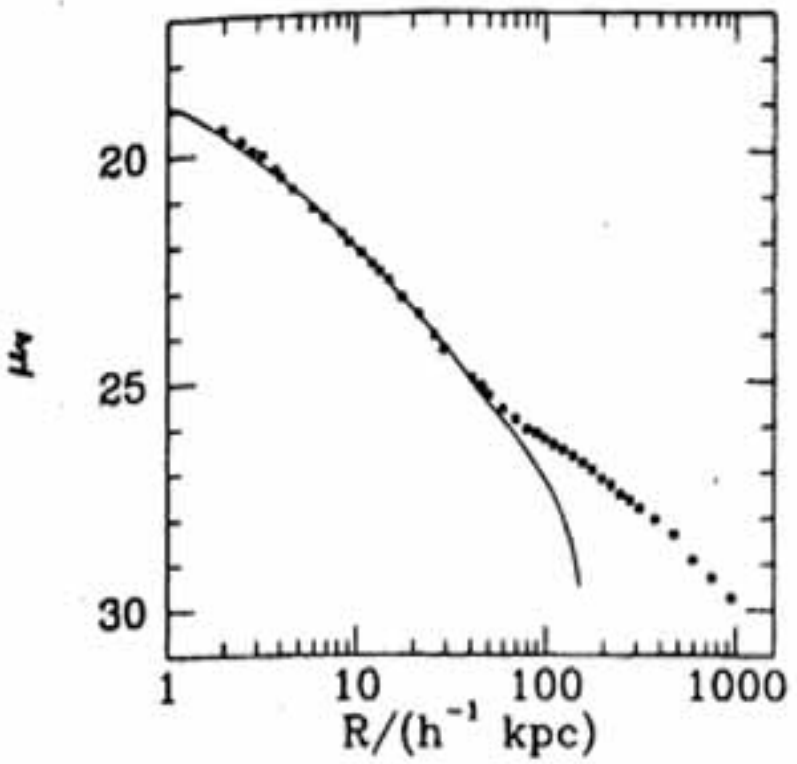

Figure 4.28 The surface-brightness profile of the cD galaxy that lies at the center of the cluster Abell 1413 (points). The line shows the $R^{1/4}$-law that best fits the inner points. [From data kindly provided by J. Schombert based on the work of Oemler (1976).]

Ellipticals with Shells

NGC 3923

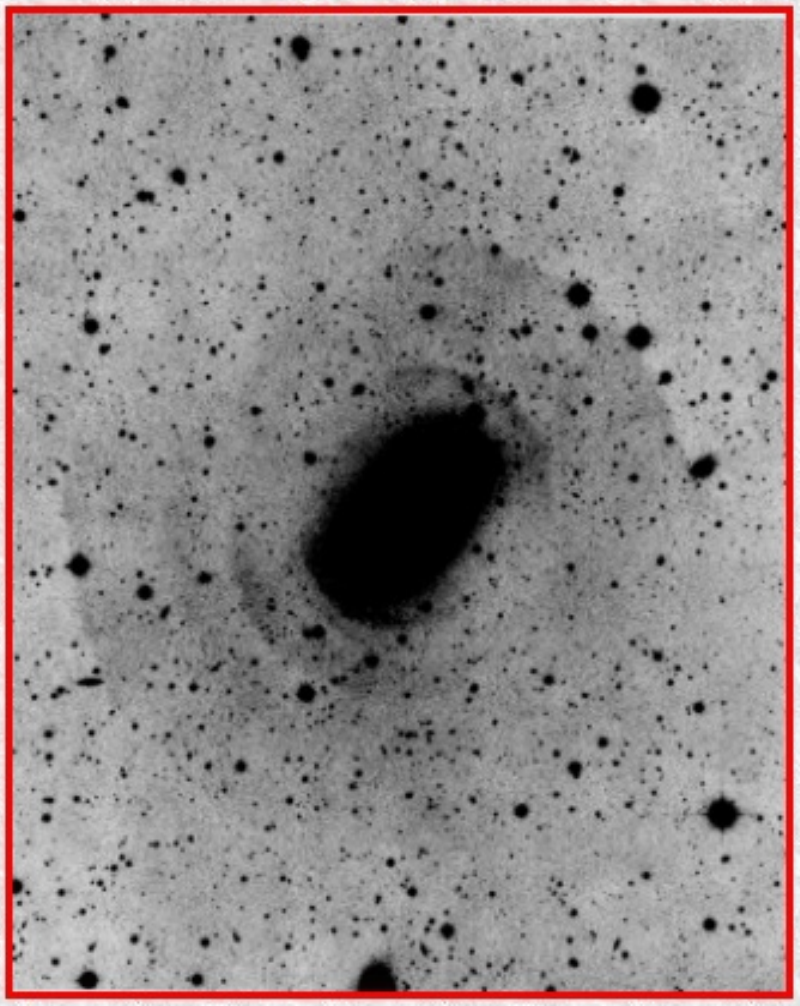

NGC 4382

(ii) Size & Luminosity vs Surface Brightness (Kormendy) Relation

A couple of correlations suggest larger, more luminous galaxies have lower surface brightness

$\langle I_e \rangle$ correlates with R_e : Kormendy Relation

- $R_e \propto \langle I_e \rangle^{-0.83 +/- 0.08}$

$\langle I_e \rangle$ correlates with L_{tot} :

- $L_{tot} \propto \langle I_e \rangle^{-2/3}$
- this follows from the above relation, given $L_e = 1/2\ L_{tot} = \pi \langle I_e \rangle R_e^2$

We conclude: larger and more luminous galaxies are **fluffier** with **lower densities**
An interpretation is not yet too clear, though galaxy formation models must explain it.
One inference: low-luminosity ellipticals formed with more gaseous dissipation than giant ellipticals.

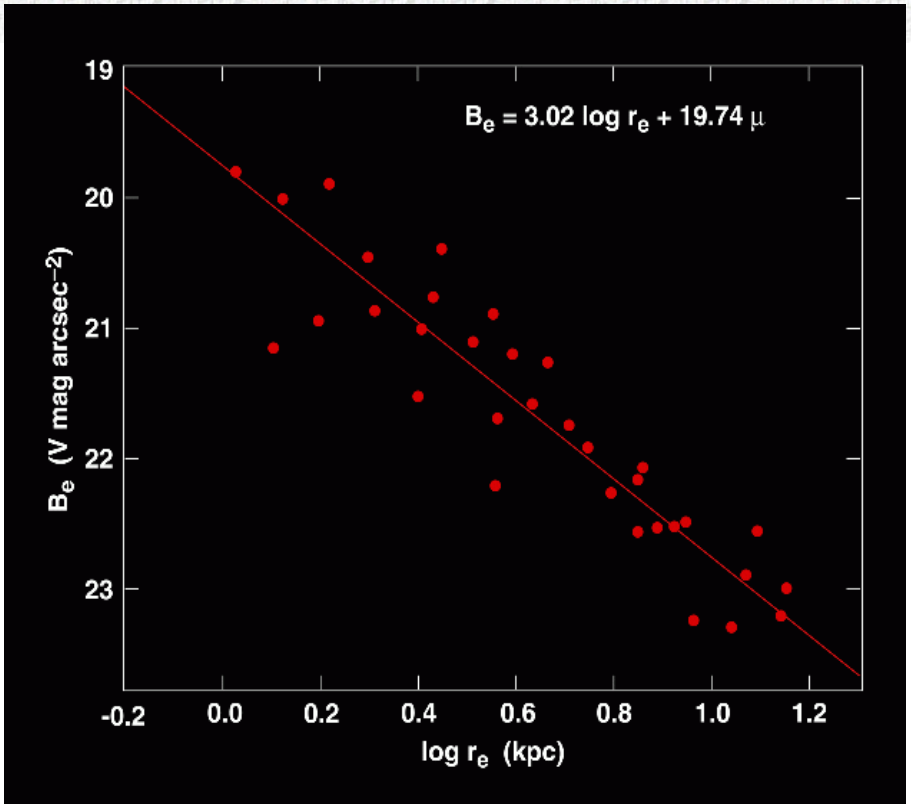

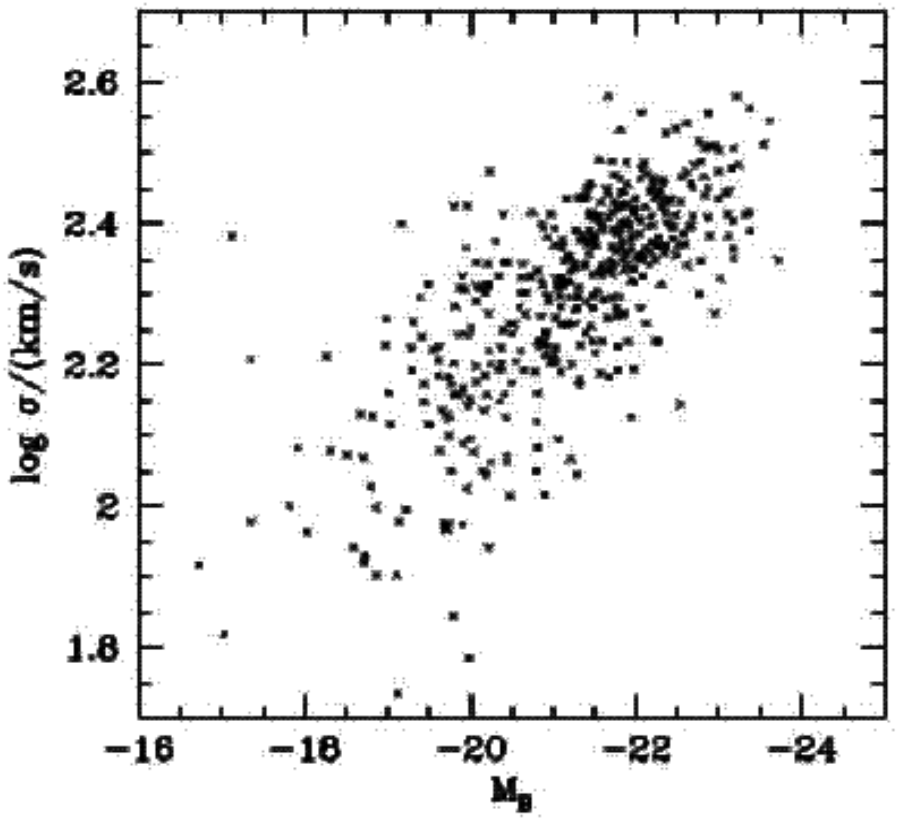

Faber-Jackson relation between central velocity dispersion and total magnitude of elliptical galaxies

$$L_B \propto \sigma^4$$

(b) The 3-Parameter Fundamental Plane

The above 2-parameter correlations have considerable **real scatter**
Furthermore, the residuals in one plot correlate with those in another.
This suggests we look for a tighter correlation among **three** parameters:

- A tilted **plane** of points in 3-D volume, which
- Projects onto 2-D planes as the (looser) correlations seen above
- One example is: $\text{Log } R_e = a \text{ Log } \sigma + b \text{ Log } I_e + c$

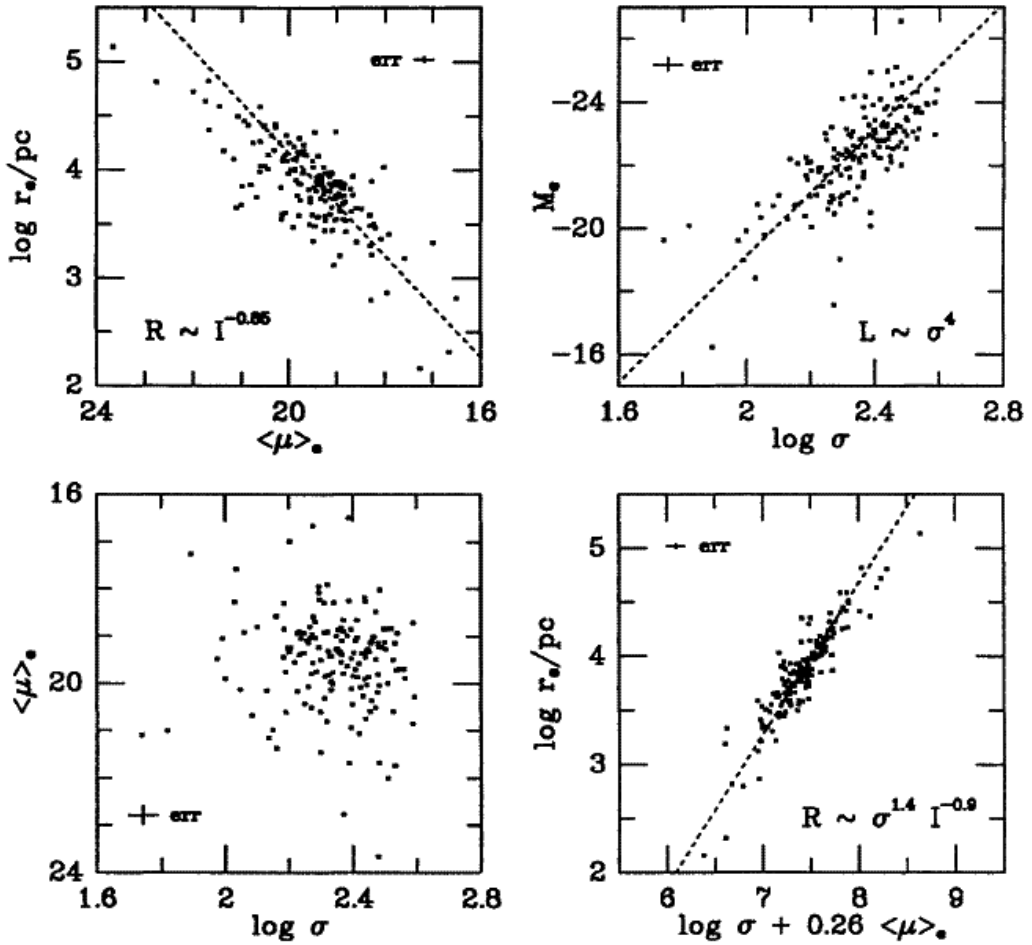

Figure 2 Projections of the fundamental parameter plane of elliptical galaxies. *Top panels*:

(iv) The Physical Basis of the Fundamental Plane

The following gives some insight into the origin of the F-P relation :
Consider:

- $\langle I_e \rangle = \frac{1}{2} L_{tot} / \pi R_e^2$ (just a definition)
- $M/R_e = c \sigma_e^2$ (virial equilibrium, KE $\propto$ PE; c = "structure parameter" containing all details)

Taken together, these give:

- $R_e = (c/2\pi) (M/L)^{-1} \sigma_e^2 \langle I_e \rangle^{-1}$ or equivalently,
- $\text{Log } R_e = \text{Log } [(c/2\pi) (M/L)^{-1}] + 2 \text{Log } \sigma_e - \text{Log} \langle I_e \rangle$ or
- $\text{Log } R_e = \text{Log } [(c/2\pi) (M/L)^{-1}] + 2 \text{Log } \sigma_e + 0.4 \langle \mu_e \rangle$ (since $\langle \mu_e \rangle = -2.5 \text{Log} \langle I_e \rangle$)

So, **if** c and M/L are constants, then we expect

- $\text{Log } R_e = 2 \text{Log } \sigma_e + 0.4 \langle \mu_e \rangle + \text{Log } [(c/2\pi) (M/L)^{-1}]$

Which is **close to**, but not quite, the F-P relation:

- $\text{Log } R_e = 1.4 \text{Log } \sigma_e + 0.36 \langle \mu_e \rangle + \text{const}$

To bring these into agreement, we require:

- $(2\pi/c) (M/L) \propto M^{1/5} \propto L^{1/4}$

Color-Magnitude Relation

Abell 2218

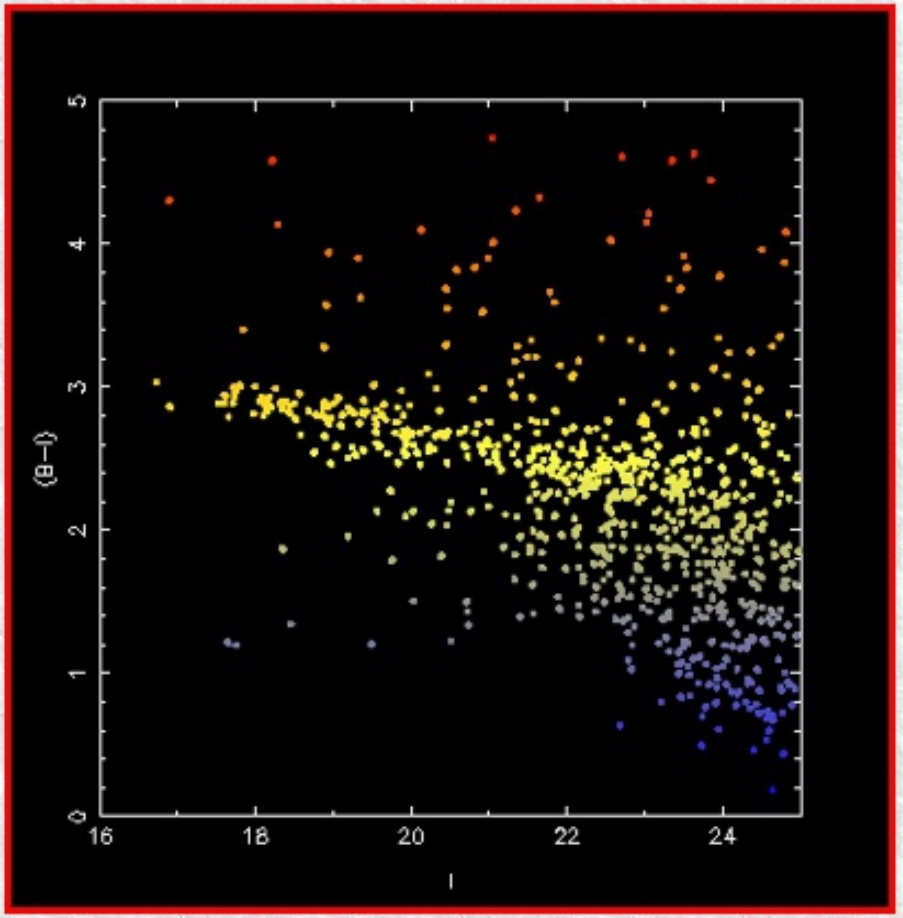

Abell 2218

Colors and magnitude for galaxies in the field of Abell 2218. Many fain background galaxies are included, but the primary early-type color-magnitude strip is clearly visible.

Metallicity vs Velocity Dispersion

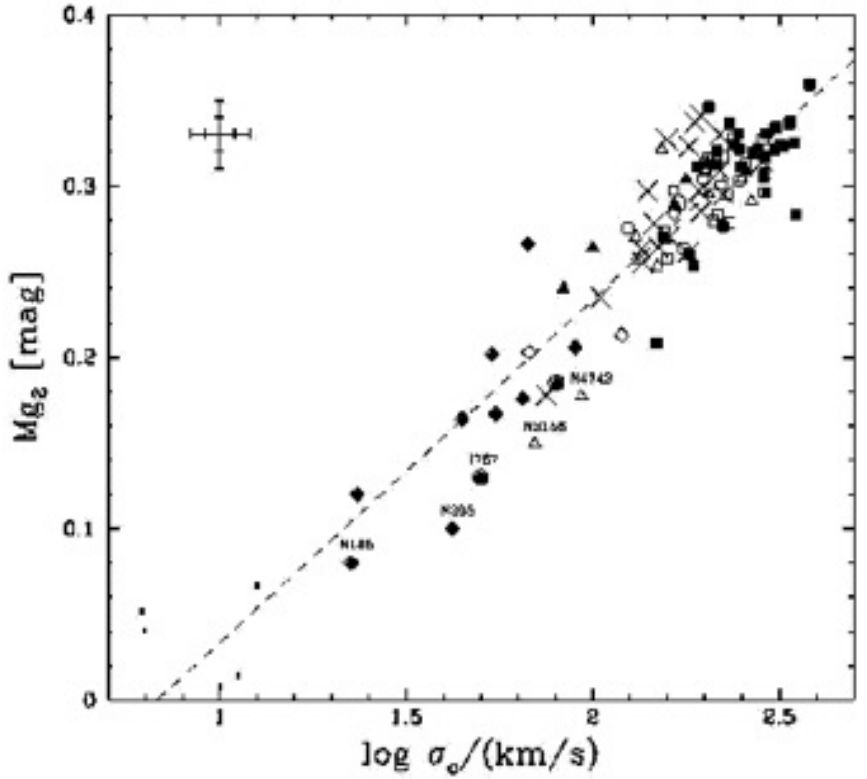

Relationship between Mg_2 and σ_o for ellipticals (squares), S0 bulges (crosses), dwarf ellipticals (diamonds and small squares), special objects (open squares).
(Bender, IAU Symp 149)

Mg2 metallicity index increases in Ellipticals (and S0 bulges) of higher velocity dispersion.

Remnants of simulations of the merger of two equal mass galaxies

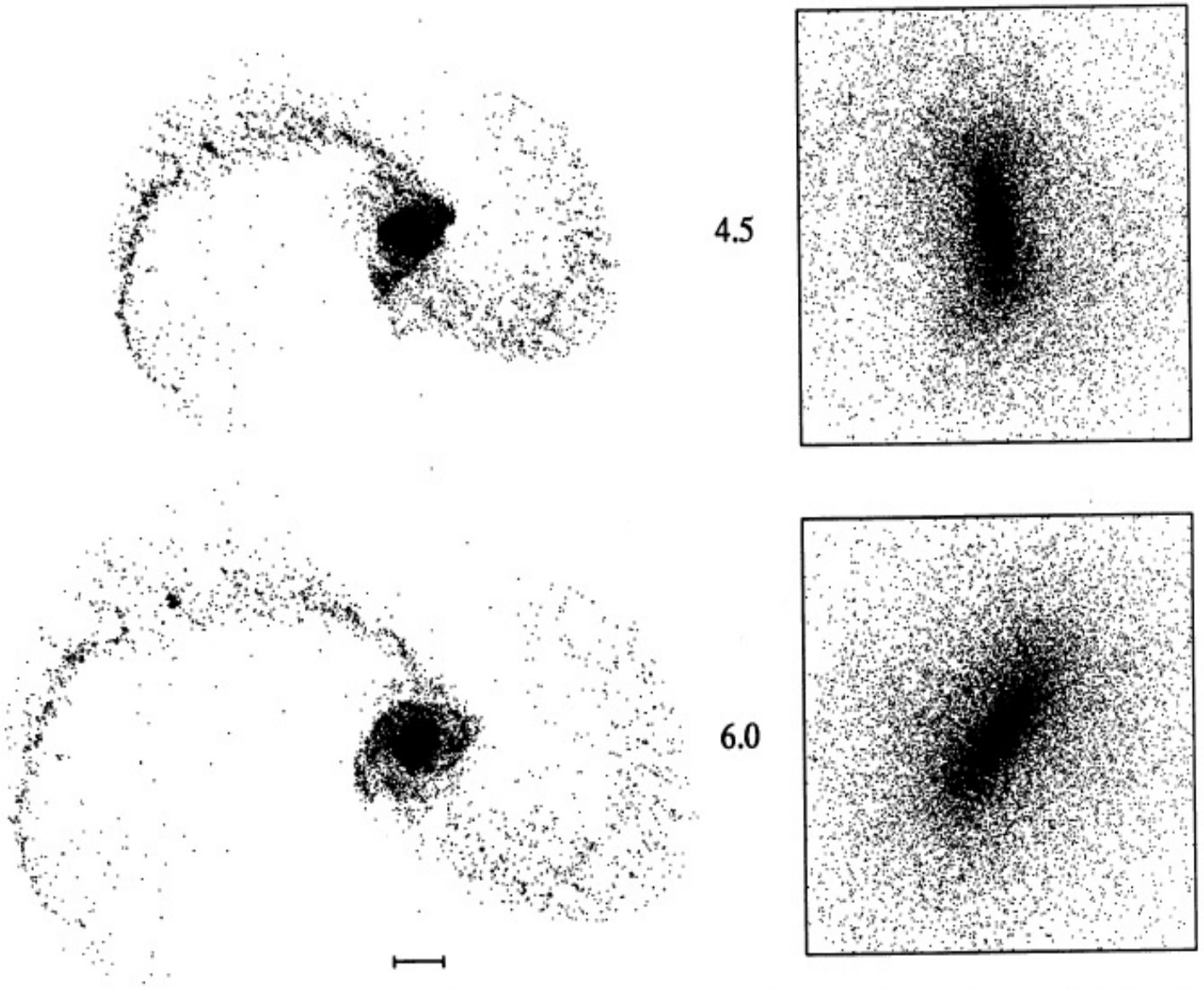

FIG. 11.—Large-scale (*left*) and small-scale (*right*) structure of the merger remnant in encounter **A**, projected onto the orbital plane, at times 3, 4.5, and 6. The boxes, enlarged by a factor of 10 from their unframed counterparts, are 0.8 × 0.8 length units. Again, only 50% of the bulge particles are plotted.

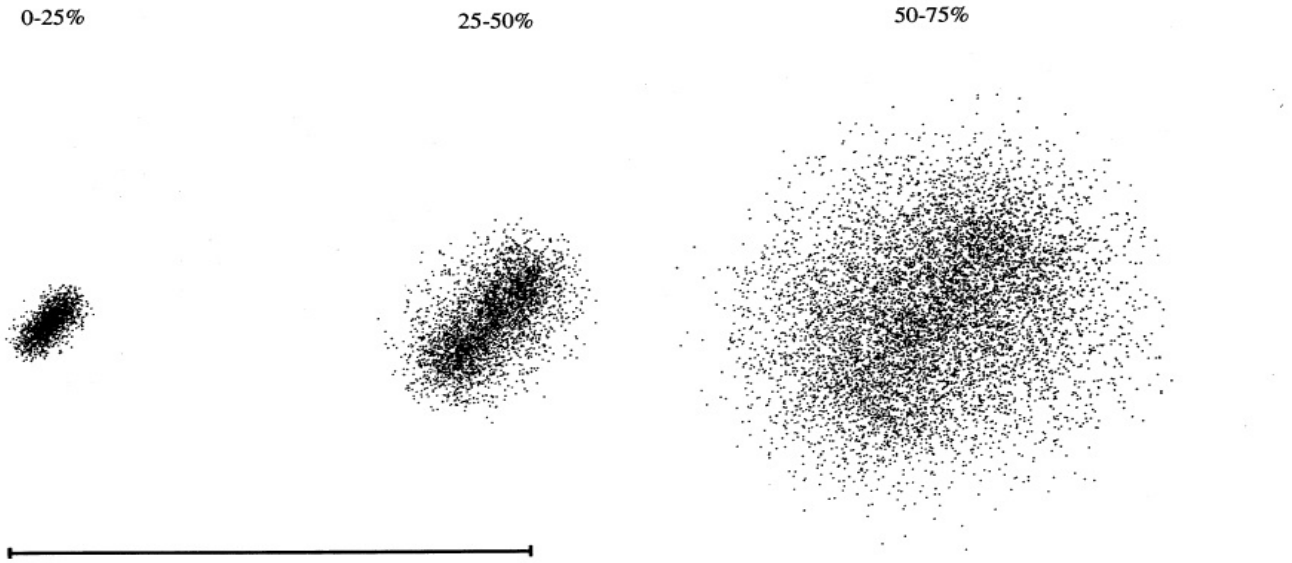

FIG. 15.—Luminous particles from the remnant produced by encounter A at time $t = 6$, binned by their specific binding energy. On the left is the 0%–25% bin, thinned by a factor of 4 to reduce crowding. In the middle is the 25%–50% bin, thinned by a factor of 2. On the right is the 50%

Original profile

After merging

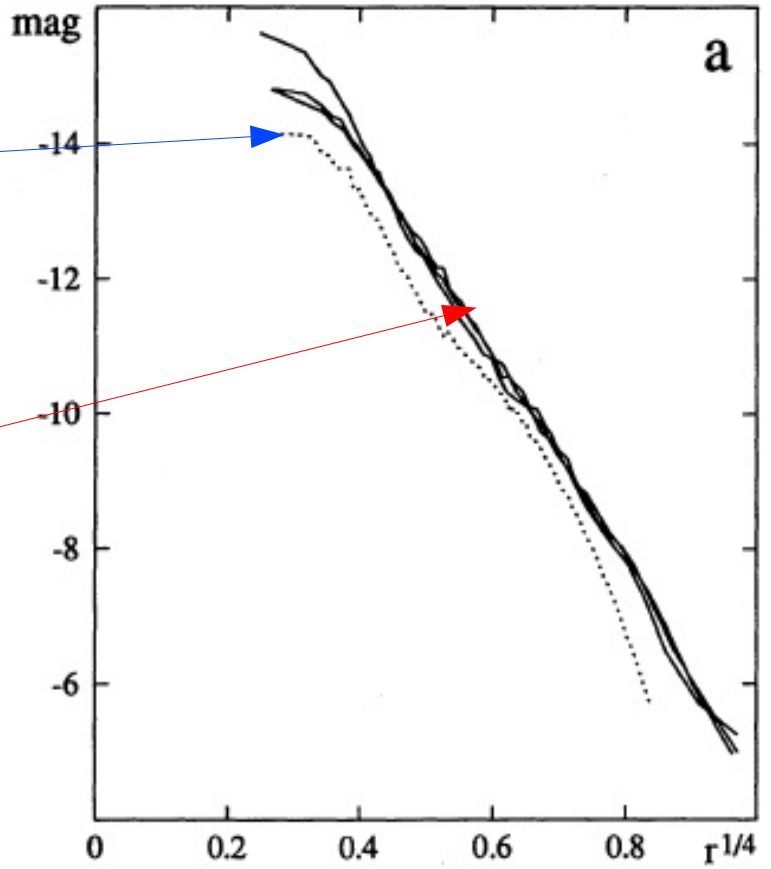

Major mergers with gas

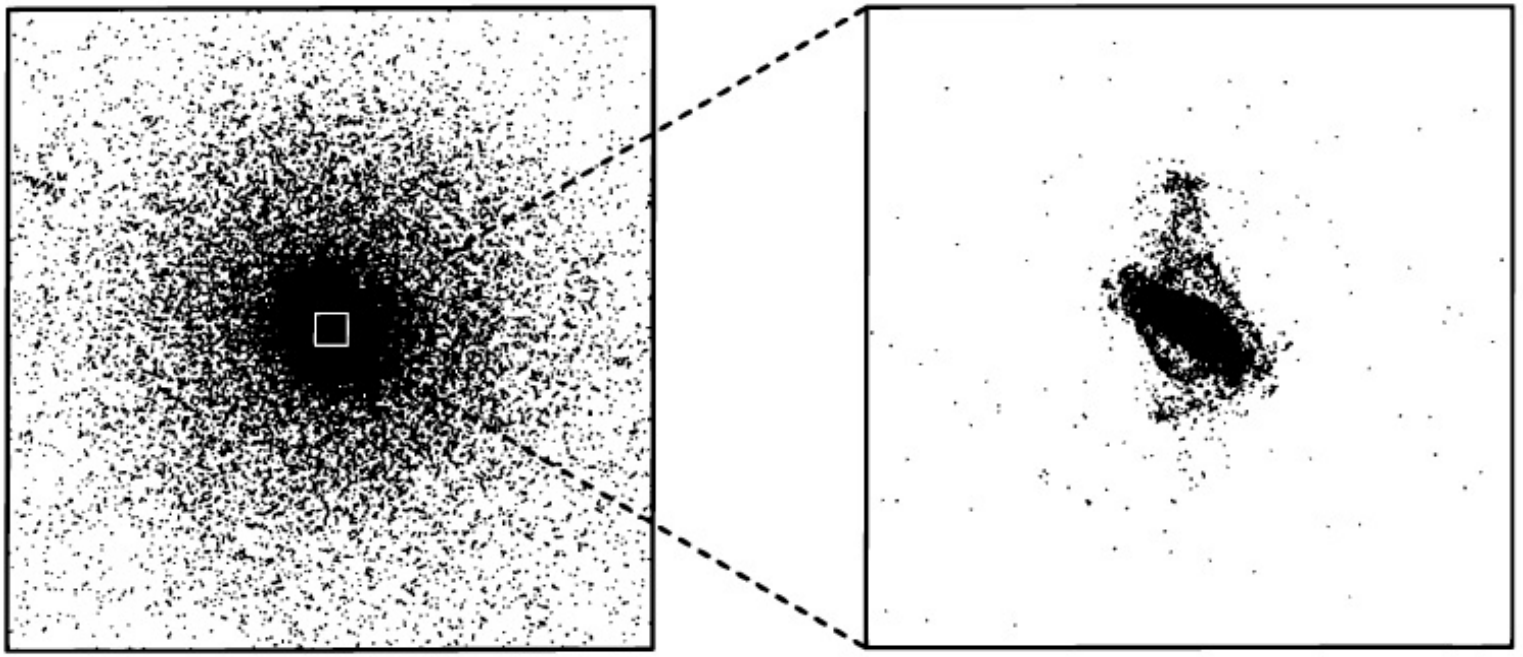

FIG. 14.—Views of stars (*left*) and gas (*right*) in the merger remnant produced by encounter A at time $t = 6$. The stellar view is 0.8×0.8 length units, while the view of the gas is enlarged by a factor of 20. Over 60% of all the gas in this remnant lies in this dense central blob.

Formation of elliptical galaxies in a cosmological context

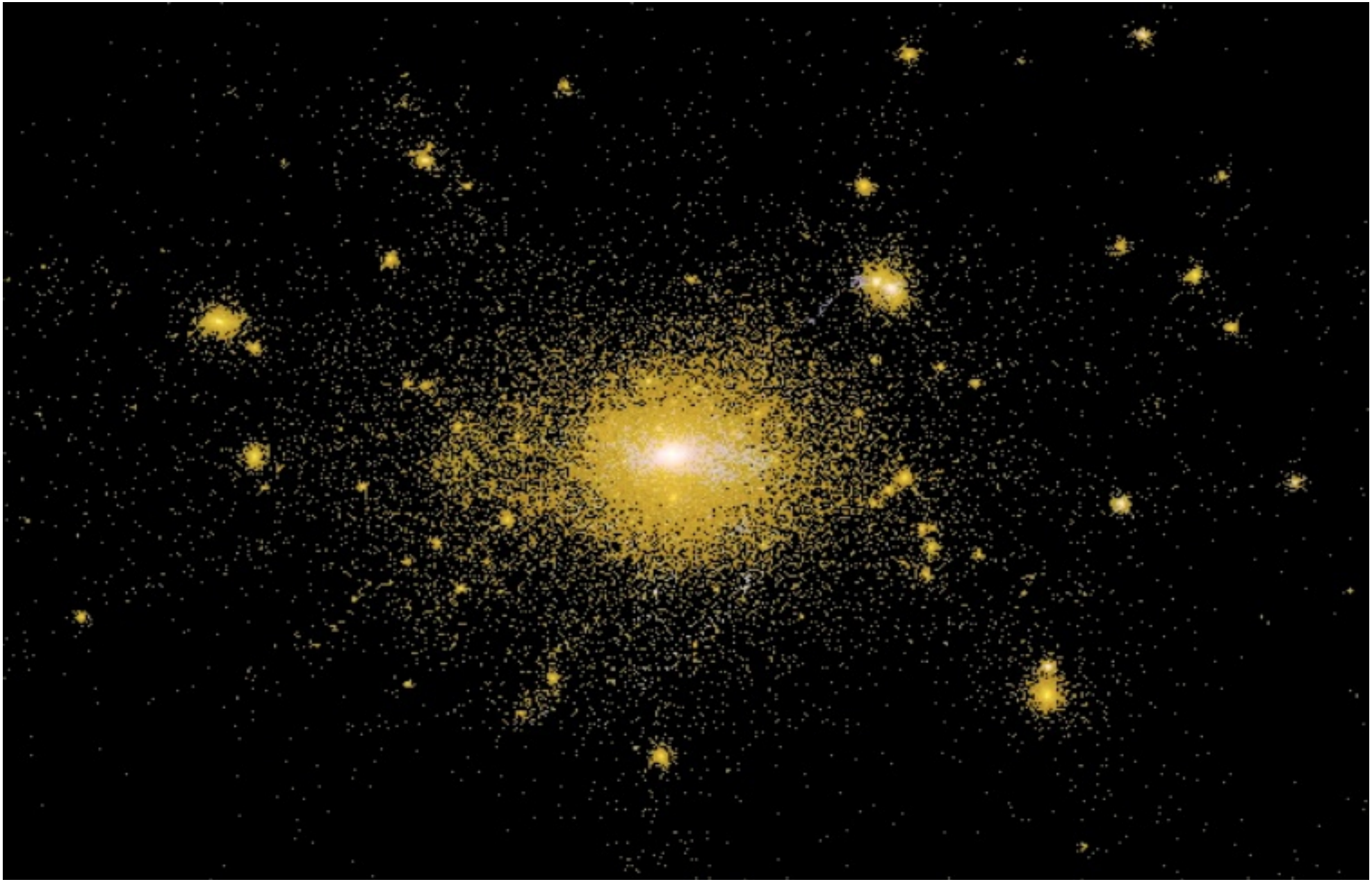

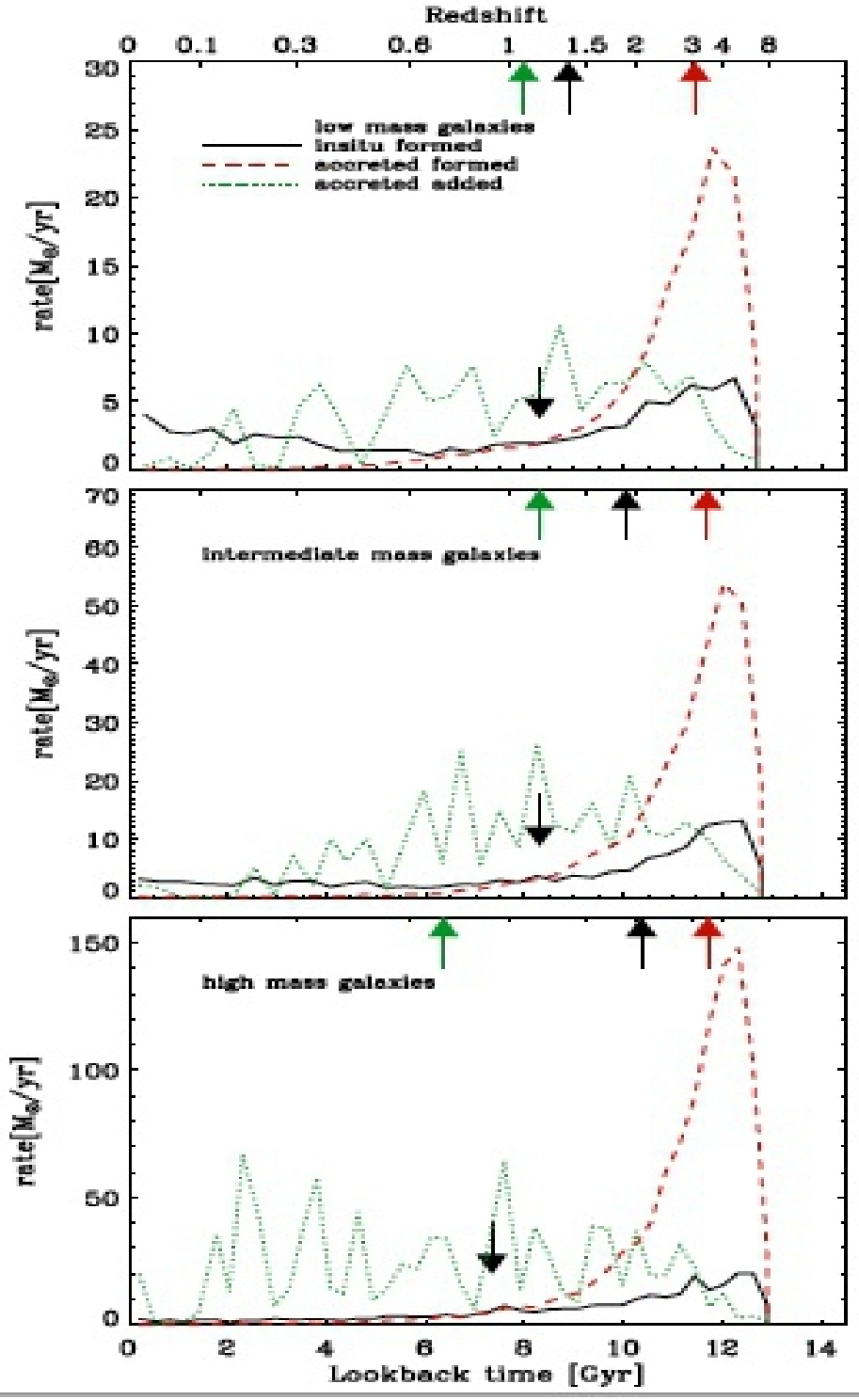

"In situ formed": stars formed from cooling gas in central galaxy

"In situ accreted formed": star formed from gas accreted by central galaxy in merging satellites.

"Accreted added": stars added by merging satellites

Two-phase model

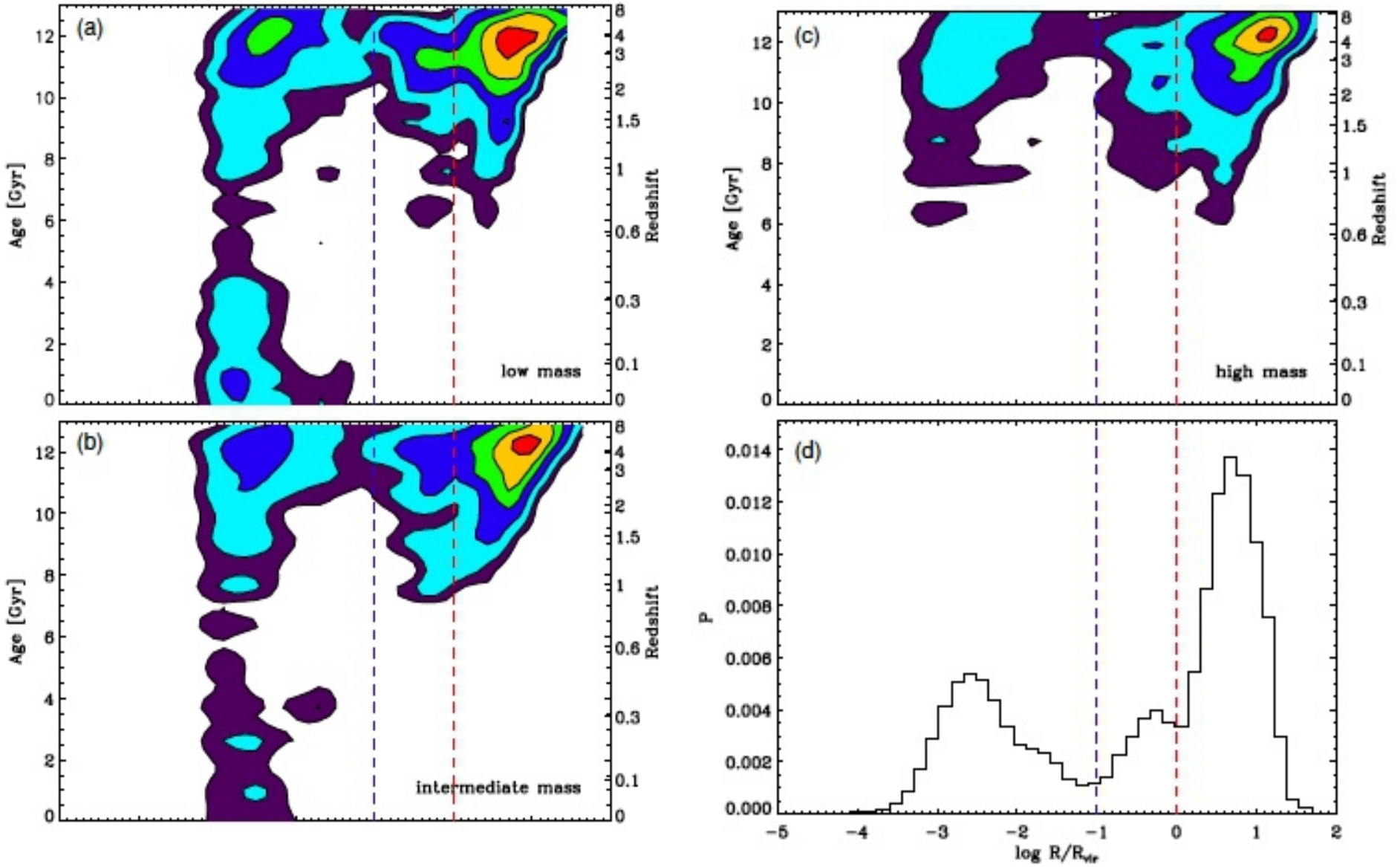

log R/R_{vir}

Size-mass relation at different redshifts

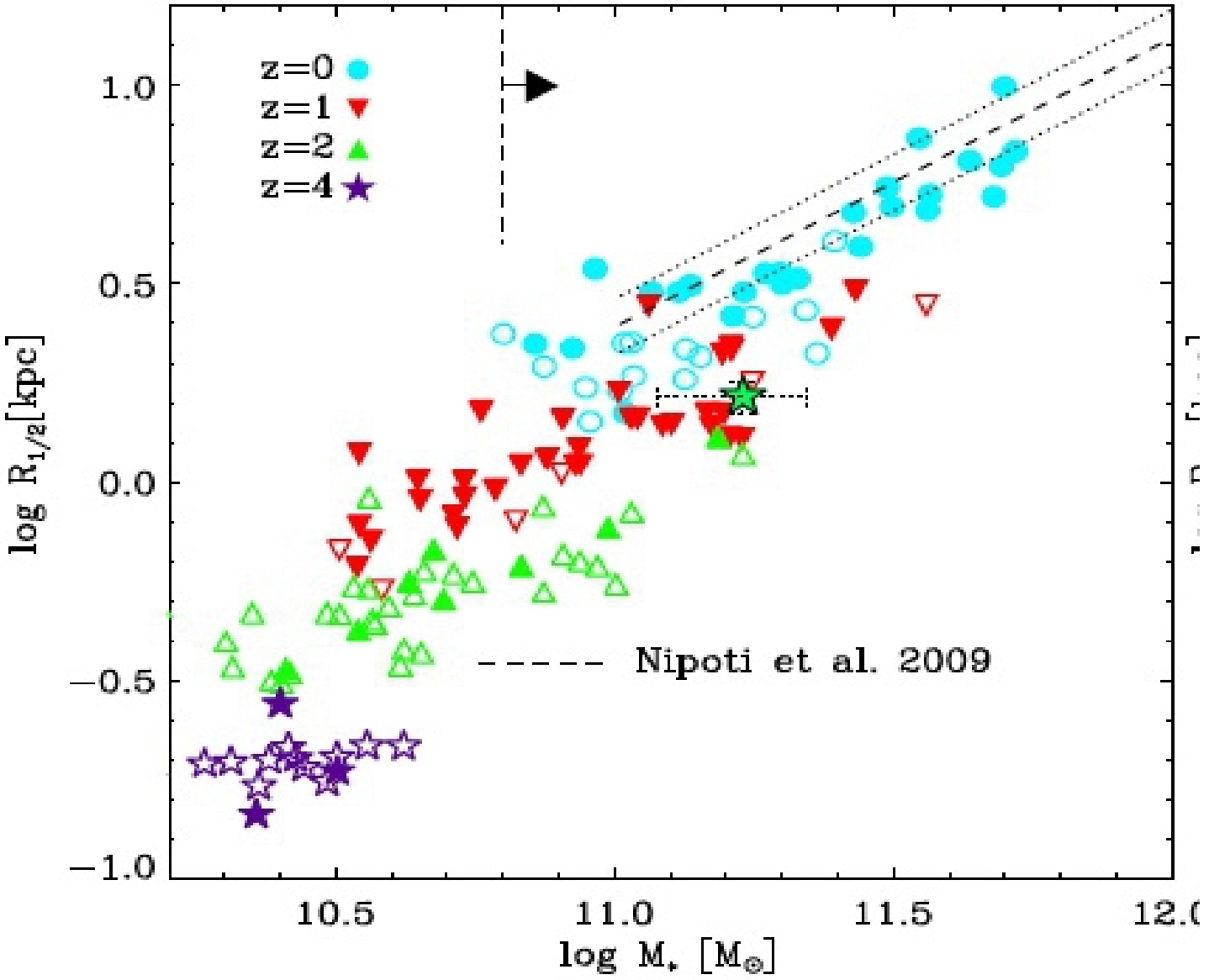

Velocity dispersion-mass relation